Spring net community production and its coupling with the CO_2 dynamics in the surface water of the northern Gulf of Mexico

Zong-Pei Jiang[1,2], Wei-Jun Cai[2*], John Lehrter[3], Baoshan Chen[2], Zhangxian Ouyang[2], Chenfeng Le[1], Brian J. Roberts[4]

5   [1]Ocean College, Zhejiang University, Zhoushan, Zhejiang, China
[2]School of Marine Science and Policy, University of Delaware, Newark, Delaware, USA
[3]University of South Alabama, Alabama, USA
[4]Louisiana Universities Marine Consortium, Louisiana, USA

Correspondence to: Wei-Jun Cai (wcai@udel.edu)

10   **Abstract.** Net community production (NCP) in the surface mixed layer of the northern Gulf of Mexico (nGOM) and its coupling with the CO_2 system were examined during the productive spring season. NCP was estimated using multiple approaches: 1) underway O_2 and Ar ratio, 2) light/dark bottle oxygen incubations, and 3) non-conservative changes in dissolved inorganic carbon and nutrients; in order to assess uncertainties and compare the temporal-spatial scales associated with the different approaches. NCP estimates derived from various methods showed similar pattern along the river-ocean

15   mixing gradient. The NCP_{O2Ar} estimated from the high resolution O_2 and Ar underway measurement is characterized by negative rates (-25.4 mmol C m^{-2} d^{-1}) at the high nutrient and high turbidity river end (salinity<5) resulting from light limitation and the influence of terrestrial carbon input. NCP_{O2Ar} had highest rates (up to 235 mmol C m^{-2} d^{-1}) in the river plume regions at intermediate salinities between 15 to 30 where light and nutrient were both favorable for phytoplankton production. NCP_{O2Ar} rates were much lower (1.2 mmol C m^{-2} d^{-1}) in high salinity (salinity>31) oligotrophic offshore waters

20   due to nutrient limitation. Air-sea CO_2 fluxes generally showed corresponding changes from being a strong CO_2 source in the river channel to a CO_2 sink in the plume. CO_2 fluxes were near zero in offshore waters indicating balanced autotrophy and heterotrophy at these sites. Overall, the surface water in the nGOM (93-89.25°W, 28.5-29.5°N) was strongly autotrophic during the spring season in spring 2017 with mean NCP rate of 21.2 mmol C m^{-2} d^{-1} and as a CO_2 sink of -6.7 mmol C m^{-2} d^{-1}. By using a 1-D model, we demonstrated that a temporal mismatch between in situ biological production and gas exchange

25   of O_2 and CO_2 could result in decoupling between NCP and CO_2 flux (e.g., autotropic water as a CO_2 source outside the Mississippi river mouth and heterotopic water as a CO_2 sink near the Atchafalaya Delta). This decoupling was a result of in situ biological production superimposed on the lingering background pCO_2 from the source water because of the slow air-sea CO_2 exchange rate and buffering effect of the carbonate system.

1 Introduction

The continental shelf is among the most biologically active areas of the biosphere and plays a significant role in global

biogeochemical cycles (Chen and Borges 2009; Chen and Swaney 2012; Gattuso et al. 1998; Muller-Karger et al. 2005).

Despite its moderate surface area (~7%), the continental shelf accounts for 14-30% of net ecosystem production, 80% of

5   organic matter burial (Gattuso et al. 1998), and 15-21% of the CO_2 uptake of the global ocean (Cai 2011; Cai et al. 2006;

Chen and Borges 2009; Laruelle et al. 2010). Moreover, anthropogenic impacts have substantially changed the nutrient and

carbon delivered to the coastal oceans (Bauer et al. 2013; Regnier et al. 2013; Yang et al. 2018), with associated

development of a series of environmental problems, e.g., coastal eutrophication, hypoxia, and acidification (Cai et al. 2011;

Diaz and Rosenberg 2008; Rabalais et al. 2014; Wallace et al. 2014). Understanding and quantifying how these impacts

10   affect the metabolic balance and CO_2 fluxes of coastal systems is of critical interest to scientists and policy-makers. However,

the substantial heterogeneity resulting from physical and biogeochemical interactions makes assessing trophic state and

carbon flux a challenging task in dynamic coastal environments.

Net community production (NCP) is defined as the difference between gross primary production and community respiration

(Eppley and Peterson 1979; Sarmiento and Gruber 2006). NCP reflects the trophic state of the aquatic ecosystem indicating

15   whether the ecosystem is a net source or sink of organic matter (Eppley and Peterson 1979; Sarmiento and Gruber 2006).

NCP in the mixed layer plays an important role in regulating the surface CO_2 and O_2 dynamics. It also represents the amount

of organic carbon available for export to subsurface, which is closely related to bottom water biogeochemical processes, e.g.,

the development and maintenance of hypoxia.

The northern Gulf of Mexico (nGOM) is a river-dominated continental shelf (Mckee et al. 2004) which receives a large

20   amount of carbon and nutrient inputs from the Mississippi-Atchafalaya River system (Lohrenz et al. 2014). NCP and CO_2

dynamics in the nGOM are significantly affected by the concurrent terrestrial inputs of nutrients and carbon loadings. The

CO_2 variability and air-sea CO_2 flux in the nGOM have been extensively investigated by high resolution underway

measurement of the partial pressure of CO_2 (pCO_2) (Huang et al. 2015). High terrestrial inorganic and organic carbon

loading results in CO_2 over-saturation and net CO_2 efflux to the atmosphere in the lower river channel and estuary of the

25   Mississippi River (Cai 2003; Guo et al. 2012; Huang et al. 2015; Lohrenz et al. 2010). On the continental shelf, reduced

$p\text{CO}_2$ observed at moderate salinities in the Mississippi plume (sink for atmospheric CO_2) was attributed to strong primary production supported by the excessive riverine nutrient loads (Guo et al. 2012; Huang et al. 2015; Lohrenz et al. 1990; 1999; 2014). With the enhanced surface production and subsequently subsurface respiration of the sinking organic matter, recurring bottom hypoxia that covers large portions of the Louisiana-Texas shelf has been observed in summer when

5   stratification limits O_2 replenishment (Bianchi et al. 2010; Obenour et al. 2013; Rabalais et al. 2002). Springtime riverine nutrient flux and subsequent biological production in surface waters play a critical role in determining the size of the summertime bottom-water hypoxia area in the nGOM (Justić et al. 1993; Turner et al. 2012). The rapid subsurface respiration also leads to significant decrease in pH and a weakening of acid-base buffer capacity, which leads to the enhanced coastal ocean acidification problem (Cai et al. 2011).

10   However, the detailed relationship between NCP and CO_2 dynamics in the surface water in the nGOM remains unclear because of the low spatial resolution of the conventional NCP measurements based on discrete samples (Guo et al. 2012, Huang et al. 2012, Cai 2003). In this study, we present high resolution NCP estimates from continuous measurement of O_2 to Ar ratio in the nGOM in spring 2017. These rates were compared to NCP estimates derived from traditional approaches (light/dark bottle oxygen incubation and non-conservative removal of DIC and nutrients). The simultaneous underway

15   determination of NCP_{O2Ar} and $p\text{CO}_2$, together with measurements of dissolved oxygen (DO), DIC, total alkalinity (TA), nutrients and other environmental parameters, allow us to better constrain the variability and controls of the metabolic balance and CO_2 flux in the nGOM. We also use a 1-D model to investigate the relationship between NCP and air-sea fluxes of O_2 and CO_2. In particular, we demonstrate that there is a time lag between surface NCP and air-sea CO_2 exchange due to the buffering of CO_2 within the carbonate system, which results in a decoupling between NCP and CO_2 flux.

20   **2 Methods**

2.1 Sample collection and measurements

The study region covers the Mississippi and Atchafalaya river estuary and the adjacent Louisiana continental shelf (Fig. 1). Sampling of this region was conducted onboard the *RV Pelican* during 6-16 April 2017. At 83 sampling stations vertical water column profiles of temperature, salinity, DO, chlorophyll fluorescence (Chl-a), and photosynthetically available

radiation (PAR) were measured by a SeaBird SBE 911plus system. Discrete water samples were collected 3-12 depths

depending on the bottom depth and the vertical salinity and O_2 structures of the water reading from the SBE 911plus profiler.

Samples for DIC and TA were collected in 250 mL borosilicate glass bottles and preserved with 50 µl of saturated $HgCl_2$

solution (Dickson et al. 2007). DIC was measured by non-dispersive infrared measurement on the CO_2 stripped from the

5   acidified sample (AS-C3, Apollo SciTech. USA). TA titrations were conducted with a ROSS™ combination electrode 8102

(Thermo Fisher Scientific) on an automated titrator (AS-ALK2, Apollo SciTech). DIC and TA measurements were

calibrated with certified reference materials provided by A. G. Dickson, Scripps Institution of Oceanography. The precision

and accuracy of the DIC and TA measurements were better than 0.1% (~2 µmol kg^{-1}) (Huang et al. 2012). River water

samples of the Mississippi (89.98°W, 29.85°N) and Atchafalaya (91.21°W, 29.70°N) were taken on 5 April, one day prior to

10   the cruise, to identify the DIC and TA concentrations of the river end members. DO was measured by a Shimadzu UV-1700

at 25°C using the spectrophotometric method following Pai et al. (1993). For nutrient analysis, water from each Niskin bottle

was immediately filtered through 0.22 µm, sterile, polyethersulfone (PES) syringe filters and stored frozen for subsequent

nutrient characterization. Samples were analyzed in duplicate for dissolved NO_x (NO_3^- + NO_2^-) by Cu-Cd reduction followed

by azo dye colorimetry using a Lachat Instruments QuikChem® FIA+ 8000 Series Automated Ion Analyzer with an ASX-

15   400 Series XYZ autosampler at the Louisiana Universities Marine Consortium as described previously (Roberts and Doty

2015).

2.2 Underway measurements

The underway system was fed by the ship's seawater supply from an inlet located at an approximate depth of ~3 m. The

flow-through system and the Multiple Instrument Data Acquisition System (MIDAS) provide sea surface temperature,

20   conductivity (Seabird SBE 21 Thermosalinograph), chlorophyll fluorescence (Turner Model 10 Series Fluorometers), and

light transmittance (WETLabs 25-centimeter path length transmissometer). MIDAS also integrates data from the ship's

meteorological suite: wind, barometric pressure, temperature and relative humidity (R.M. Young) and photosynthetically

active radiation (LI-COR LI-190SZ).

Underway seawater pCO$_2$ was measured by an automated flow-through pCO$_2$ measuring system (AS-P2, Apollo SciTech)

25   with a shower head equilibrator and a non-dispersive infrared gas detector (LI-COR, LI-7000) (Huang et al. 2015). The

underway pCO$_2$ system alternates measurements on a stream of seawater split from the same inlet for MIDAS and a stream

of outside air from the bow of the vessel away from the chimney contamination. The atmospheric pCO$_2$ was measured every

3h automatically. The pCO$_2$ measurement was calibrated regularly against 3 certified gas standards (150.62, 404.72, 992.54

ppm) and has an accuracy of 2 µatm. The underway DO was measured by an Aanderaa 4835 optode which was calibrated

5   against discrete spectrophotometric measurements.

Underway high-resolution measurements of oxygen to argon ratio (O$_2$/Ar) were made by an Equilibrator Inlet Mass

Spectrometry as described by Cassar et al. (2009). Briefly, a fraction of underway seawater (the same supplied to the pCO$_2$

system) was pumped through a gas-permeable membrane contactor cartridge at a flow rate of 100 mL min^{-1}. The cartridge is

connected to a quadrupole mass spectrometer (Pfeiffer Prisma) through a fused-silica capillary which continuously samples

10   headspace gases for O$_2$/Ar ratio measurements. Calibrations of the O$_2$/Ar ion current ratio were conducted by sampling the

ambient air every 3 hours through a second capillary. The instrument precision is ±0.3% or better (Cassar et al. 2009).

2.3 Calculations

The mixed layer depth (MLD) was defined as the depth at which the density changes by 0.03 kg m^{-3} relative to the surface

value and was calculated according to the density profiles at sampling stations. Air-sea CO$_2$ flux was calculated as:

15   $$F_{CO2} = k_{CO2}\, K_0 \left(p\mathrm{CO}_{2sea} - p\mathrm{CO}_{2air} \right) \quad (1)$$

where k$_{CO2}$ is the gas transfer velocity of CO$_2$ calculated using the daily mean wind speed from the three-dimensional

Coupled Ocean/Atmosphere Mesoscale Prediction System (COAMPS) (Hodur 1997) and the coefficients of Sweeney et al.

(2007). The COAMPS daily wind speed agreed well (mean difference = 0.4 m s^{-1}) with the measurements from the buoys in

our study region (s42047, s8768094, FRWL1, MRSL1, LOPL1, GISL1, PSTL1, PILL1, data from the National Data Buoy

20   Center, http://www.ndbc.noaa.gov/maps/WestGulf.shtml). K$_0$ is the CO$_2$ solubility coefficient calculated from temperature

and salinity (Weiss 1974). pCO$_{2sea}$ and pCO$_{2air}$ are the observed pCO$_2$ concentrations in the surface ocean and in the

atmosphere respectively. Comparing to the large variations in pCO$_{2sea}$ (110-1800 µatm), the variability of pCO$_{2air}$ (pCO$_{2air}$ =

405 ± 4 µatm) was minor and the pCO$_{2air}$ is set at a uniform value as the mean observed concentration for the flux

calculation. The negative F$_{CO2}$ corresponds to a net CO$_2$ influx (ocean as CO$_2$ sink for the atmosphere). The pCO$_2$ buffer

factor response to change in DIC (γ_{DIC}) is calculated following Egleston et al. (2010) and Álvarez et al. (2014). High γ_{DIC} indicates strong buffering capacity and small change in pCO$_2$ for a given change in DIC.

Air-sea O$_2$ flux was calculated as:

$$\mathrm{F_{O2}} = k_{O2}\left(\mathrm{O_{2sea}} - \mathrm{O_{2sat}}\right) \quad (2)$$

5   where k_{O2} is the gas exchange velocity of O$_2$ which is calculated in a similar way with that of k_{CO2}. The percentage saturation of DO (DO%) is calculated as DO%=O$_{2sea}$/O$_{2sat}$, where O$_{2sea}$ is the observed seawater DO concentration and O$_{2sat}$ is the saturated DO concentration (Garcia and Gordon 1992).

2.4 NCP estimates

In this study, mixed layer average NCP rates were estimated by four different approaches: underway O$_2$/Ar measurements

10   (NCP$_{O2Ar}$), light/dark bottle DO incubations (NCP$_{DO-incub}$), and non-conservative changes in DIC (NCP$_{\Delta DIC}$) and NO$_x$ (NCP$_{\Delta NOx}$).

NCP from the O$_2$/Ar method: The surface NCP can be estimated from the O$_2$/Ar measurements through an oxygen mass balance in the mixed layer under a steady state assumption, refer to Kaiser et al. (2005) and Cassar et al. (2011) for details. As shown in Fig. 2, DO concentration in the surface water is affected by physical (e.g., changes in temperature, salinity and

15   atmospheric pressure, bubble dissolution and/or injection) and biological processes (photosynthesis and respiration). Ar and O$_2$ have similar responses to the physical processes as they have similar solubility and temperature dependency (Garcia and Gordon 1992; Hamme and Emerson 2004). On the other hand, Ar is biologically inert and can be used to infer abiotic influences on oxygen ([O$_2$]$_{phys}$). Contemporaneous measures of O$_2$ and Ar thus allows the biological-induced O$_2$ changes ([O$_2$]$_{biol}$) to be isolated (Craig and Hayward 1987):

20    $$[\mathrm{O_2}]_{biol} = [\mathrm{O_2}] - [\mathrm{O_2}]_{phys} \approx [\mathrm{O_2}] - \frac{[\mathrm{Ar}]}{[\mathrm{Ar}]_{sat}}[\mathrm{O_2}]_{sat} = \Delta(\mathrm{O_2}/\mathrm{Ar})\frac{[\mathrm{Ar}]}{[\mathrm{Ar}]_{sat}}[\mathrm{O_2}]_{sat} \quad (3)$$

where [O$_2$] and [Ar] are the O$_2$ and Ar concentrations of the seawater sample, [O$_2$]$_{sat}$ and [Ar]$_{sat}$ are the equilibrium saturation concentrations (Garcia and Gordon 1992; Hamme and Emerson 2004), and Δ(O$_2$/Ar) is the biologically mediated oxygen supersaturation (Cassar et al. 2011).

$$\Delta(O_2/Ar) = \frac{[O_2]/[Ar]}{[O_2]_{sat}/[Ar]_{sat}} - 1 \quad (4)$$

If the influences of vertical mixing and lateral advection are neglected, the budget of the $[O_2]_{biol}$ in mixed layer can be described as (Kaiser et al. 2005):

$$MLD \frac{d[O_2]_{biol}}{dt} = NCP - k_{O2} \frac{[Ar]}{[Ar]_{sat}} [O_2]_{sat} \Delta(O_2/Ar) \quad (5)$$

5   where the second term on the right represents O_2 gas exchange supported by net community production (Fig. 2). Under a physically isolated assumption, NCP can be approximated by the net air-sea biological oxygen flux (bioflux) (Jonsson et al. 2013):

$$NCP_{O2Ar} = bioflux = k_{O2}[O_2]_{sat} \Delta(O_2/Ar), \quad NCP \text{ unit: } (mmol \ O_2 \ m^{-2} \ d^{-1}) \quad (6)$$

where k_{O2} was calculated from the 10-m COAMPS wind speed (Hodur 1997) following the wind speed-dependent

10   parameterization of Sweeney et al. (2007). The weighting technique of Reuer et al. (2007) modified by Teeter et al. (2018) was applied to account for the 30-day wind speed history prior to the arrival of ship. Here Ar is assumed to be at equilibrium saturation ($[Ar]/[Ar]_{sat} = 1$ in Eq. 5), which introduces an error of ~1% into NCP estimate (Cassar et al. 2011). The modeling study by Teeter et al. (2018) suggested that the bioflux accurately represents the exponentially weighted NCP over the past several residence times of O_2. The residence times of O_2 (MLD/gas transfer velocity of O_2, ~2.3 days during our cruise)

15   refers to the length of time required to exchange O_2 between the mixed layer and the atmosphere (Kaiser et al. 2005; Teeter et al. 2018).

NCP from the DO incubation: NCP was estimated with bottle incubations at 43 CTD stations (Fig. 1). Water samples were collected from Niskin bottles into triplicate clear and black 300-ml BOD bottles (Wheaton). The initial DO saturation and temperature in each bottle was measured by inserting a luminescent/optical dissolved oxygen probe (Hach LDO101, Hach

20   Hq40d meter) into the bottle. Care was taken to avoid introducing air bubbles during this step. After recording the initial saturation value, the probe was removed and the small volume (3-5 ml) displaced by the probe was replaced with filtered seawater from an offshore, low nutrient site. The bottles were then capped with glass stoppers and placed in a deck incubator plumbed with flowing sea water from the MIDAS system in order to maintain surface water temperatures. Clear bottles were placed into boxes screened at 50% of ambient sunlight. After 24 hours, the oxygen saturation and temperature were

measured again with the oxygen probe. O_2 concentrations obtained from the LDO probe method were verified by comparison to O_2 concentrations measured by the spectrophotometric method of Pai et al. (1993) in a subset of samples. No bias was observed between the two methods.

The rate of DO change (mmol O_2 m^{-3} d^{-1}) during an incubation was calculated from the difference in DO concentrations

5   between the final and initial measurement. Respiration was calculated from the DO change rate in the dark bottles (R_{DOdark}). The integrated respiration over the MLD (mmol O_2 m^{-2} d^{-1}) was calculated as $Resp_{Int} = R_{DOdark}*MLD$. Gross primary production was calculated as $GPP = R_{DOlight} + |R_{DOdark}|$, where $R_{DOlight}$ is the average change in O_2 in the light bottles. The GPP measured at 50% light in the incubations was considered the maximum light-dependent GPP rate. The mean percentage of PAR (%PAR) in relation to surface PAR (E_0) was calculated at each station as:

10   $$\%PAR = \frac{E_0}{K_d MLD}(1 - e^{(-K_d MLD)}) \quad (7)$$

where E_0 is 100%, light attenuation (K_d, m^{-1}) is the rate of exponential decline in PAR as a function of depth as measured by the CTD. To calculate the integrated GPP in the mixed layer (GPP_{Int}, mmol O_2 m^{-2} d^{-1}), the GPP was scaled by the light environment in the MLD:

if $\%PAR \geq 50$, $GPP_{Int} = GPP*MLD$ (8)

15   if $\%PAR < 50$, $GPP_{Int} = 2*\%PAR*GPP*MLD$ (9)

The Eq. 9 assumed that GPP was linearly dependent on light up to a maximum GPP that occurred when %PAR = 50. Finally, the NCP integrated over the MLD ($NCP_{DO-incub}$) was estimated as:

$NCP_{DO-incub} = (GPP_{Int} - Resp_{Int})$, NCP unit: mmol O_2 m^{-2} d^{-1} (10)

NCP from the non-conservative changes in DIC and nutrients: NCP can also be estimated from the biological-induced DIC

20   and nutrient deficit from the conservative mixing. We applied a three end-member mixing model (Huang et al. 2012) to distinguish the concentration from conservative mixing (X_{Mix}) and the biological-induced changes (ΔX_{biol}). The X_{Mix} is calculated from the fractions of gulf seawater (f_{sw}), Mississippi River water (f_{MR}), and Atchafalaya River water (f_{AR}) together with the corresponding end-member concentrations shown in Table 1:

$1 = f_{sw} + f_{MR} + f_{AR}$ (11)

25   $X_{Mix} = X_{sw}*f_{sw} + X_{MR}*f_{MR} + X_{AR}*f_{AR}$ (12)

Here we used salinity and potential alkalinity ($PTA=TA+NO_x$) (Brewer and Goldman 1976) as the two conservative tracers

to constrain f_{sw}, f_{MR}, and f_{AR} using a non-negative least square method (Lawson and Hanson 1974). The minor contribution

of calcification to changes in TA can be ignored as in Guo et al. (2012) and Huang et al. (2012). The concentrations of

DIC_{Mix} and NO_{xMix} from conservative mixing can be calculated from Eq. 12, then the biological-induced changes in DIC

5   (ΔDIC_{NCP}) and NO_x (ΔNO_{xNCP}) can be estimated as:

$$\Delta DIC_{NCP} = DIC_{obs} - DIC_{Mix} \quad (13)$$

$$\Delta NO_{xNCP} = NO_{xobs} - NO_{xMix} \quad (14)$$

where DIC_{obs} and NO_{xobs} are the observed concentrations of DIC and NO_x. Note that ΔDIC_{NCP} (mmol C m^{-3}) and ΔNO_{xNCP}

(mmol N m^{-3}) represent the cumulative NCP-induced changes in the concentrations of DIC and NO_x since the mixing of

10   river water with oceanic water. In order to calculate the NCP rate, the MLD and plume residence time (τ) need to be

considered (Cai 2003):

$$NCP_{\Delta DIC} = \Delta DIC_{NCP}*MLD/\tau, \quad NCP \text{ unit: mmol C m}^{-2} \text{ d}^{-1} \quad (15)$$

$$NCP_{\Delta NOx} = \Delta NO_{xNCP}*MLD/\tau, \quad NCP \text{ unit: mmol N m}^{-2} \text{ d}^{-1} \quad (16)$$

In order to facilitate comparison with previous studies (Guo et al. 2012, Huang et al. 2012, Cai 2003), τ for the Mississippi

15   plume were taken from Green et al. (2006) as: 1, 1.5, 6 days for salinities 0-18, 18-27, 27-34.5 respectively. In our study, we

only calculated $NCP_{\Delta DIC}$ and $NCP_{\Delta NOx}$ for stations near the Mississippi Delta (Fig. 1) because τ for the Atchafalaya plume is

not available.

To facilitate comparison, we converted NCP estimates from different approaches (Eqs. 6, 10, 15 and 16) to the same unit in

term of carbon (mmol C m^{-2} d^{-1}) using the Redfield ratio of C:N:O$_2$ = 106:16:138. The photosynthetic molar ratio of C:O$_2$ for

20   new and recycled production may vary between 1.1 (NH$_4^+$ as nitrogen source) and 1.4 (NO$_3^-$ as nitrogen source) (Laws

1991). In our study region, the riverine input of NO$_3^-$ (Table 1) is the main nitrogen source for biological uptake and we

considered the average Redfield ratio of C:O$_2$ =106:138 to be appropriate. Although the stoichiometry of C:N may differ

from the Redfield ratio (Geider and La Roche 2002; Sambrotto et al. 1993), the applicability of the Redfield C:N ratio in our

study region has been proved (Huang et al. 2012; Xue et al. 2015; also the result of this study).

3 Results

3.1 General pattern

The discharges and NO_x loadings of the Mississippi River and Atchafalaya River exhibit typical seasonality with peaks in spring (Fig. S1). The discharge in April 2017 is slightly lower than the monthly mean value during 1997-2017 while the NO_x

5   loading is similar with the long-term average (Fig. S1). Surface water parameters (temperature, salinity, light, Chl-a, DO%, pCO_2, and $\Delta O_2/Ar$) consistently showed high spatial variability on the inner and middle shelf (bottom depth <50m), while much lower spatial variability was observed on the outer shelf and the open gulf (bottom depth >50m) (Fig. 3). The MLD was generally shallow during our study period (2-11 m) and the surface stratification was mainly caused by the buoyancy of freshwater on top of the oceanic water (Fig. 3b, c). Low light transmittance (high turbidity) was observed in the Mississippi

10   river estuary and in the coastal water at 90.5-92.3°W outside the Atchafalaya Bay (Fig. 3d). High Chl-a concentrations were generally observed in nearshore mid-salinity waters and decreased offshore (Fig. 3e). Corresponding to the high Chl-a concentrations around the Mississippi Delta, high DO% and $\Delta(O_2/Ar)$ were observed together with low pCO_2 (Fig. 3). Whereas, undersaturated DO% and negative values of $\Delta(O_2/Ar)$ were observed in the high Chl-a coastal water outside the Atchafalaya Bay at 90.5-92.3°W.

15   The highest physical and biogeochemical variations were observed in adjacent to the Mississippi South Pass during Apr. 8-10 and in the Atchafalaya coastal region during Apr. 15-17 (Figs. 3, 4). Clearly, the variability in the surface water was significantly affected by the riverine influences of Mississippi and Atchafalaya. In spring when river discharge is high and wind is typically downwelling-favorable, the Mississippi River freshwater and associated nutrient and carbon load generally flows westward toward the Texas coast in a contained nearshore current (Zhang et al. 2012; Lehrter et al. 2013). Our three

20   end-member mixing model accurately reproduced the westward extension of the Mississippi freshwater on the Louisiana shelf from the Mississippi Southwest Pass (Fig. 3b, Fig. 5a), which was similar to the non-summer pattern of the Mississippi downcoast freshwater transport modeled by Zhang et al. (2012) (Fig. 5c). Our model also suggested a westward Atchafalaya plume trajectory in a narrow band along the coast, and little Atchafalaya freshwater was transported upcoast toward the Mississippi Delta (Fig. 5b). This pattern also agreed well with the simulation result of Zhang et al. (2012) during non-

25   summer seasons (Fig. 5d). Although the coastal water outside the Atchafalaya Bay (90.5-92.3°W, region 2 in Fig. 5a) was

affected by the Mississippi freshwater (Fig. 5a), its properties were significantly different from those of the Mississippi

plume around the Mississippi Delta (Fig. 3). In comparison to the Mississippi plume, this high-turbidity Atchafalaya coastal

water (named as HTACW hereafter) was characterized by higher temperature, deeper MLD, lower light transmittance, lower

DO% and lower $\Delta O_2/Ar$ (Fig. 3). The vertical SBE 911plus profiles showed that the water column in the HTACW was well

5   mixed. Therefore, the HTACW cannot be simply treated as an extension of the Mississippi plume. To better investigate the

distribution and variability of the surface water parameters, we divided the coastal region into three sub-regions (Fig. 5a, b):

(1) the Mississippi plume (to the east of 90.5°W), (2) the HTACW (90.5-92.3°W), and (3) the Atchafalaya plume (92.3-

93.5°W along the coast).

3.2 Estimates of NCP

10   As shown in Fig. 1, $NCP_{\Delta DIC}$ and $NCP_{\Delta NOx}$ were only available at 30 stations in the Mississippi plume; $NCP_{DO\text{-}incub}$ estimates

were generated via incubation experiments at 43 stations throughout the sampling region; while the underway O_2/Ar

measurements provided NCP estimates with the highest resolution (3800 3-minute averaged rates) and most complete spatial

coverage. The $NCP_{DO\text{-}incub}$, $NCP_{\Delta DIC}$ and $NCP_{\Delta NOx}$ were mostly obtained at salinities higher than 20, while the NCP_{O2Ar}

covered the whole salinity range (0 to 36.4) providing more information of the NCP variability in the dynamic estuary

15   environments (Fig. 4). The $NCP_{DO\text{-}incub}$ (-56 to 361 mmol C m^{-2} d^{-1}) gave the highest estimate of the maximum NCP rates in

the nGOM (Fig. 4c). The results of $NCP_{\Delta DIC}$ (-19 to 275 mmol C m^{-2} d^{-1}) and $NCP_{\Delta NOx}$ (2 to 314 mmol C m^{-2} d^{-1}) in the

Mississippi plume were close to each other and their ranges were similar to that of the O_2/Ar approach (-124 to 235 mmol C

m^{-2} d^{-1}) (Fig. 4c). Acknowledging the diverging estimates from different approaches (Fig. 4c), $NCP_{DO\text{-}incub}$, $NCP_{\Delta DIC}$,

$NCP_{\Delta NOx}$ and NCP_{O2Ar} all displayed similar spatial pattern in the Mississippi plume with high production rates around the

20   Mississippi bird's foot delta (Fig. 6a-d). In the high salinity offshore waters, $NCP_{DO\text{-}incub}$ and NCP_{O2Ar} both suggested low

NCP rates close to zero (Fig. 4c, Fig. 6a, b). One major difference in $NCP_{DO\text{-}incub}$ and NCP_{O2Ar} is that O_2/Ar measurement

generated negative NCP estimates in the Mississippi river channel and in the HTACW while $NCP_{DO\text{-}incub}$ suggested positive

NCP rates in these regions (Fig. 6a, b).

3.3 Mississippi plume

In the shallow, well-mixed Mississippi river channel, the light transmittance was close to zero and the Chl-a concentrations were low despite the ample nutrient availability (NO_x up to 118 µmol/kg, Figs. 7, 8). High pCO_2 (up to 1800 µatm, Fig. 7c), under-saturated DO (~82%, Fig. 7d, 8b) and net CO_2 efflux (Fig. 7e, 8d) was observed in the Mississippi river channel,

5 which is similar to most inner estuaries (Borges and Abril 2011; Chen et al. 2012; Chen and Swaney 2012). The negative values of NCP_{O2Ar} suggested net heterotrophic condition in the inner Mississippi estuaries while the positive $NCP_{DO-incub}$ suggested net autotrophic production by the plankton community (Fig. 7f, 8c).

With the increasing light transmittance in conjunction with persistence of riverine-derived nutrient concentrations along the Mississippi plume flow path (Fig. 7a, 8a), phytoplankton biomass reached high levels at intermediate salinities (15-30, Fig.

10 7b, 8b). This corresponded to large decreases in pCO_2 (down to 130 µatm, Fig. 7c) and strong oceanic CO_2 uptake (up to 43 mmol m^{-2} d^{-1}, Fig. 7e, 8d), as well as elevated DO% (up to 180%, Fig. 7d, 8b) and NCP rates (Fig. 7f, 8c). The observed NCP rates (e.g., up to 235 mmol C m^{-2} d^{-1} in NCP_{O2Ar}, up to 361 mmol C m^{-2} d^{-1} in $NCP_{DO-incub}$) are within the range of prior estimates for this region during spring season (-238 to 624 mmol C m^{-2} d^{-1}, Cai 2003; Guo et al. 2012; Huang et al. 2012; Lohrenz et al. 1990; Lohrenz et al. 1997; Lohrenz et al. 1999), and are among the highest in large river estuarine and shelf

15 waters (Cooley and Yager 2006; Dagg et al. 2004; Ning et al. 1988; Ternon et al. 2000). The enhanced biological production also resulted in significant removal of DIC (up to 250 µmol kg^{-1}, Fig. S2a) and nutrients (up to 35 µmol kg^{-1} in NO_x, Fig. S2b) in the mid-salinity range of the Mississippi plumes. The biological uptake ratio of NO_x and DIC (0.14 in Fig. S2c) was close to the Redfield ratio (16/106=0.15).

3.4 Atchafalaya plume and HTACW

20 The Atchafalaya River discharges in a shallow broad, low-gradient shelf (10m isobath doesn't occur until more than 40km offshore of the delta) frequently experiences cross shelf currents (Roberts and Doty 2015). The Atchafalaya plume waters, extended westward in a narrow band along the coast (region 3 in Fig 5b), generally showed similar biogeochemical variability as the Mississippi plume (Fig. 7). The observation results in the Atchafalaya plume were characterized by elevated Chl-a, DO%, and NCP at intermediate salinities coupled with dropdown in pCO_2 and oceanic CO_2 sink (Fig. 7).

Although the Chl-a concentrations in the HTACW (region 2 in Fig 5a) were similar to those in the Atchafalaya plume in the

salinity range of 25 to 30 (Fig. 7b), undersaturated DO were observed in the HTACW with low light transmittance (Fig. 7a,

d). The $p\text{CO}_2$ concentrations in the HTACW were generally higher than those in the Atchafalaya plume at the same salinities

(Fig. 7c), but the HTACW still acted as a sink for atmospheric CO_2 (Fig. 7e). Similar to that in the Mississippi river channel,

5   the two approaches for NCP estimation presented different results in the HTACW: the negative NCP_{O2Ar} rates suggest net

heterotrophy (Fig. 6a) while $NCP_{DO\text{-}incub}$ indicates net autotrophy (Fig. 6b).

4. Discussion

4.1 Comparison of NCP estimations

In our study, the NCP rates estimated from different independent approaches refer to different temporal and space scales.

10   The $NCP_{DO\text{-}incub}$ was estimated from the 24-hour DO changes in incubation bottles, which gives a snapshot of daily estimate

for the ecosystem in the water column at the sampling location. The $NCP_{\Delta DIC}$ and $NCP_{\Delta NOx}$ in the Mississippi plume

reflected the average community production rate along the flow path over the transit time of the plume water since the

beginning of river-ocean mixing process. The NCP_{O2Ar} represents the average NCP exponentially weighted over the past

several residence times of oxygen in the mixed layer along the flow path of the sampled water (Kaiser et al. 2005; Teeter et

15   al. 2018).

In addition, each approach has its independent assumptions and limitations:

NCP from the O_2/Ar method: A key assumption of the O_2/Ar method is the physically isolated condition with negligible

physical inputs. Recent studies have shown that entrainment and upwelling processes (mixing with O_2-depleted subsurface

water) can lead to significant underestimation in NCP using the O_2 budget approach, especially in areas with low biological

20   production rates and in coastal upwelling zones (Castro-Morales et al. 2013; Nicholson et al. 2012; Shadwick et al. 2015;

Teeter et al. 2018). The influence of entrainment and upwelling is expected to be minor in most areas of our study region

because of the persistent spring-summer halocline stratification (Fig. 3c). However, the contribution from benthic

metabolism in the well-mixed Mississippi river channel and the HTACW adds an additional complexity to the O_2/Ar

approach. In these well-mixed shallow waters, NCP_{O2Ar} reflected not only the NCP in the mixed layer, but the NCP in the

whole water column including the signals of benthic processes. An additional source of uncertainty in NCP_{O2Ar} is associated

with the calculation of the bioflux of O_2. Although the variable gas transfer velocity can be considered using a weighting

technique for wind speed history (Reuer et al. 2007; Teeter et al. 2018), O_2 flux calculated from different wind speed

parameterizations (Liss and Merlivat 1986; Nightingale et al. 2000; Sweeney et al. 2007; Wanninkhof 1992) could result in a

5   relative variability of 15%.

NCP from the DO incubation method: Although the DO incubation method is a direct measurement of NCP, there are

uncertainties related to scaling from samples collected at discrete depths to integrated surface mixed layer values. First, the

scaling method used here assumes a homogenous distribution of respiration rate over the MLD. Second, we only measured

GPP at one light level (50%) and we assumed that the GPP at this level was maximal and that GPP below 50% surface PAR

10   was linearly scaled to %PAR (Eqs. 8, 9). Similar assumptions for the Louisiana shelf were tested previously by Murrell and

Lehrter (2011) who found that single point measurements (vs. multi-point measurements in a layer) provided robust

estimates of integrated rates. However, in the current study, the assumption has been further applied to shallow nearshore

sites (< 10 m depth), which may exhibit greater heterogeneity due to the very high biomass and suspended sediment particles.

More importantly, the bottle incubation method accounts for the NCP by plankton community but is not able to detect the

15   impact of sediment metabolism (e.g., benthic respiration in the Mississippi river channel and the HTACW).

NCP from the non-conservative changes in DIC and nutrients: There are several sources of uncertainty associated with the

NCP estimated from the non-conservative mixing change in DIC and nutrients. Frist, errors in estimating water residence

time and MLD leads to proportional errors in the NCP estimation (Eqs. 15, 16). The plume water residence time most likely

are a function of river discharge and other physical conditions, it is therefore expected that using a set of past model-assessed

20   τ values probably would introduce the largest uncertainty in the estimation of $NCP_{\Delta DIC}$ and $NCP_{\Delta NOx}$. The varying MLD

along the flow path of the river plume would also result in large uncertainty. Second, the air-to-sea CO_2 flux in the plume

water resulted in increases in DIC concentrations which caused slight underestimation of $NCP_{\Delta DIC}$ (Eq. 13) while $NCP_{\Delta NOx}$

was not affected (Eq. 14). Third, uncertainty may be caused by the changes in the riverine concentrations of DIC and

nutrients. However, this uncertainty decreases with salinity (Huang et al. 2012) and was generally low in our study.

Considering the different temporal and spatial resolutions and uncertainties associated with different approaches, a

comparison of NCP estimated from various methods should be interpreted with caution (Ulfsbo et al. 2014). In the

Mississippi plume, all methods showed strong heterogeneity in the dynamics Mississippi plume regions (Fig. 6a-d, 8c). For

instance, the NCP rates varied significantly within the salinity range of 26 to 28 (-17 to 361 mmol C m^{-2} d^{-1} for $NCP_{DO-incub}$, -

5 7 to 192 mmol C m^{-2} d^{-1} for NCP_{ADIC}, 8 to 232 mmol C m^{-2} d^{-1} for NCP_{O2Ar}). The study of Teeter et al. (2018) showed that

NCP_{O2Ar} could be a poor estimate of daily production rate (e.g., $NCP_{DO-incub}$ in our study) when the mixed layer is not at

steady state. Meanwhile, NCP_{O2Ar} is less able to capture episodic extremes due to the inherent averaging of the O_2/Ar

approach. These could explain the observed difference between NCP_{O2Ar} and $NCP_{DO-incub}$ in the dynamic Mississippi plume.

The major difference between NCP_{O2Ar} and $NCP_{DO-incub}$ is that $NCP_{DO-incub}$ suggested autotrophy in the Mississippi river

10 channel and in the HTACW where NCP_{O2Ar} suggested heterotrophy (Fig. 6a-b, 8c). These nearshore waters were

characterized by well-mixed water column which indicates that the surface O_2/Ar could be affected by vertical mixing with

sub-pycnocline waters and benthic metabolism. In these well-mixed waters, the DO incubation approach accounted for the

plankton production in the mixed layer while the NCP_{O2Ar} approach reflected the NCP of the whole water column including

the benthic signals. On one hand, production in the mixed layer only represented a fraction of the total production of the

15 water column as the euphotic depth commonly extended below the pycnocline and sub-pycnocline chlorophyll maxima were

frequently observed in the nGOM (Lehrter et al. 2009). The study by Lehrter et al. (2009) suggested a substantial faction

(25-50%) of phytoplankton production occurs beneath the pycnocline. On the other hand, high sediment oxygen

consumption and bottom water plankton community respiration rates were observed on the Louisiana continental shelf

(Murrell et al. 2013). By comparing rates of water column primary productivity and community respiration, Murrell et al.

20 (2013) showed shelf scale net heterotrophy metabolism for the whole water column on the Louisiana shelf. Therefore, the

different results from $NCP_{DO-incub}$ and NCP_{O2Ar} in the Mississippi river channel and the HTACW were not contradictory:

$NCP_{DO-incub}$ suggested autotrophic production of the plankton community in these nearshore waters while NCP_{O2Ar} indicated

net heterotrophy metabolism for the whole water column mainly resulting from benthic respiration. As the underway O_2/Ar

method provides the highest resolution NCP estimation coupled with pCO_2 measurement, NCP_{O2Ar} was presented together

with the CO_2 variables in the following sections to investigate the variability and controls of the metabolic balance in the

nGOM.

4.2 Controls on the surface NCP and CO_2 flux

Nutrients, irradiance, and mixing were considered to be the major controlling factors of biological production in the nGOM

5   coastal waters (Lehrter et al. 2009; Lohrenz et al. 1999; Murrell et al. 2013; Turner and Rabalais 2013). Here we used the

observation results from the Mississippi plume (Fig. 8) to demonstrate the controlling mechanisms of the surface NCP and

CO_2 flux in the nGOM. As shown in Fig. 8a, there is an ecological gradient along the river-ocean mixing continuum: from

high nutrient and turbid freshwater to clear, oligotrophic offshore oceanic waters. The freshwater input from the Mississippi

River was characterized by high loadings of inorganic carbon (e.g., DIC = 2312 µmol kg^{-1}, Table 1) and organic carbon

10   (Bianchi et al. 2010). In the Mississippi river channel, production of the surface plankton communitywere limited by light

availability despite the high nutrient concentration (Fig. 8a, c). Although with the autotrophic surface plankton community

(95 mmol C m^{-2} d^{-1} in NCP$_{DO-incub}$), the whole water column in the Mississippi river channel was heterotrophic (indicated by

the negative NCP$_{O2Ar}$ rates of -51 mmol C m^{-2} d^{-1}, Fig. 8c). This was mainly caused by benthic respiration enhanced by the

decomposition of terrestrial organic carbon, but may also be related to rapid turbulent mixing and short water residence

15   times (Lehrter et al. 2009; Lohrenz et al. 1990; Lohrenz et al. 1999; Roberts and Doty 2015). The net heterotrophy at the low

salinity end corresponded to a strong CO_2 source for atmosphere (55 mmol C m^{-2} d^{-1}, Fig. 7e, 8d). Noted that although we

observed high CO_2 efflux at low salinities, its contribution to the overall regional CO_2 flux was relatively small due to its

limited spatial coverage (Huang et al., 2015).

Due to the alleviation of light limitation in conjunction with persistence of riverine nutrient concentrations, Chl-a, DO% and

20   NCP$_{O2Ar}$ all showed an increasing trend with salinity along the flow path of the Mississippi plume (Fig. 8). At intermediate

salinities (15 to 30) in the Mississippi plume, there exists an "optimal growth region" (Demaster et al. 1996) where light and

nutrient are both favorable for phytoplankton growth (Fig. 8). NCP$_{O2Ar}$ reached high level (average 105 mmol C m^{-2} d^{-1}) in

this optimal growth region corresponding to an oceanic CO_2 uptake of -13.5 mmol C m^{-2} d^{-1} (Fig. 8). We observed a positive

correlation between the averaged NCP$_{O2Ar}$ rates and Chl-a concentrations in the Mississippi plume (NCP$_{O2Ar}$ = 16.91*Chl-a -

25   35.87, R²=0.75). In high-salinity offshore water where the terrestrial influence is minor, phytoplankton growth and

16

production are primarily limited by the depleted nutrient concentration (Lehrter et al. 2009; Lohrenz et al. 1990; Lohrenz et al. 1999). DO and pCO_2 concentrations in the offshore gulf water were close to equilibrium with atmosphere and NCP_{O2Ar} rates were close to zero (Fig. 3). Overall, the study region (93-89.25°W, 28.5-29.5°N) was estimated to be net autotrophic during the study period with mean NCP_{O2Ar} rate of 21.2 mmol C m^{-2} d^{-1} and acts as a CO_2 sink of -6.7 mmol C m^{-2} d^{-1}.

5   The spatial patterns of NCP and CO_2 flux in the nGOM are associated with the trajectory of the Mississippi and Atchafalaya plumes as the surface biogeochemical variations are strongly affected by riverine influences. For instance, an unusually broad plume extension in the nGOM in March 2010, driven by upwelling favorable wind and high freshwater discharge, was associated with elevated chlorophyll concentrations and stronger biological CO_2 uptake (Huang et al. 2013). Modeling studies also suggested that NCP and CO_2 flux in the nGOM were susceptible to changes in river and wind forcing (Fennel et

10   al. 2011; Xue et al. 2016). To better study the variability of surface NCP and CO_2 flux, further studies are needed to investigate how the seasonal and inter-annual variations in environmental conditions (freshwater discharge, riverine inputs of carbon and nutrients, wind forcing, coastal circulation etc.) would affect the trajectory of the river plumes and the biological processes therein.

4.3 Coupling between NCP and CO_2 flux

15   The NCP affects air-sea gas exchange through its influence on O_{2sea} and pCO_{2sea} in seawater. Net autotrophy results in a net biological release of O_2 (increase in O_{2sea}) and uptake of CO_2 (decrease in pCO_{2sea}), while net heterotrophy has the opposite effects. As shown in Fig. 9, most NCP_{O2Ar} and CO_2 flux data collected in the Mississippi River channel fall in quadrant 2 with negative NCP rates (net heterotrophy) associated with CO_2 outgassing to the atmosphere. The Mississippi plume and Atchafalaya plume waters exhibited opposite patterns with most of the data from these regions being in quadrant 4 (Fig. 9),

20   which had positive NCP rates and a CO_2 sink for the atmosphere. This indicates strong coupling between the elevated autotrophic biological production and CO_2 uptake.

However, the air-sea pCO_2 difference (ΔpCO_2) is not only affected by in situ NCP (ΔpCO_{2NCP}), but also related to the background ΔpCO_2 level ($\Delta pCO_{2background}$) which is modulated by preceding mixing and biological processes:

$\Delta pCO_2 = \Delta pCO_{2background} + \Delta pCO_{2NCP}$ (15)

25   Therefore, net autotrophy (negative ΔpCO_{2NCP}) does not necessarily result in a CO_2 uptake from the atmosphere if the NCP-

induced pCO_2 decrease occurs in a water with high positive ΔpCO_{2NCP} from previous heterotrophy. Similarly, net

heterotrophy does not necessarily result in a CO_2 outgassing if the background pCO_2 of the source water is low.

Here we used a simple 1-D model to demonstrate the relationship between NCP and air-sea gas fluxes of O_2 and CO_2. The

environmental settings of the model were taken from the averaged condition during our study period: temperature = 22°C,

5   salinity = 35, TA = 2400 μmol L^{-1}, pCO_{2air} = 405 μatm, MLD = 6 m, and wind speed = 6 m s^{-1}. The initial state of the

seawater (day 0) was set to be equilibrium with atmosphere and the concentrations of DO, DIC and pCO_2 of the seawater

were modified by the time-dependent NCP functions and gas exchange at hourly time steps. The relative changes in

concentrations of DIC, TA and DO resulting from NCP were assumed to follow the ratio of -106:17:138 (Zeebe and Wolf-

Gladrow 2001). The pCO_2 was calculated from DIC and TA using the CO2SYS program (Pierrot, and Wallace 2006). The

10 air-sea flux of O_2 and pCO_2 were calculated following Eq. 1 and Eq. 2.

In Run-1 simulation (Fig. 10), we assumed the occurrence of 30-day net autotrophic production (100 mmol C m^{-2} d^{-1}) from

day 0 to 30 as well as 30-day net heterotrophic production (-100 mmol C m^{-2} d^{-1}) from day 0 to -30 (Fig. 10a). Both for the

autotrophy and heterotrophy simulations, the air-sea O_2 flux increased rapidly reaching a balance with the NCP-induced O_2

production or consumption in a few days (Fig. 10c). The changes in seawater DO concentration resulting from NCP were

15 then counteracted by gas exchange and the DO concentration remained constant (Fig. 10b, c). This reflects the principle of

the O_2/Ar approach which uses the biologically derived O_2 flux to estimate NCP. On the other hand, the combined effects of

NCP and gas exchange resulted in constant decreases in DIC and pCO_2 during the autotrophy simulation (day 0 to day 30)

and constant increases in DIC and pCO_2 during the heterotrophy simulation (day 0 to day -30, Fig. 10b, e). Due to the lower

pCO_2 buffering capacity (γ_{DIC} in Fig. 10e) of the high-DIC water, the increasing rate of pCO_2 under the heterotrophic

20 condition is faster than that under the autotrophic condition (Fig. 10b). The DIC changes resulting from NCP and gas

exchange equals on day -30 during the heterotrophy simulation (Fig. 10d) while the autotrophy-induced DIC decreases were

constantly higher than the CO_2 influx caused by the gas exchange during the autotrophy simulation (Fig. 10b). The longer

equilibrium time of CO_2 than O_2 is related to the difference in their relative air-sea exchange rates (Fig. 10f), and, more

importantly to the carbonate buffering system, i.e., the gas exchange-induced changes in aquatic CO_2 are buffered by a much

25 larger carbon pool of $HCO_3^- - CO_3^{2-}$ (Fig. 2).

18

In Run-2 simulation (Fig. 11), we demonstrated how the preceding biological processes and the lingering background pCO_2 affect the relationship between NCP and CO_2 flux. The NCP rate in Run-2 simulation varied with time: NCP was 0 during day 0 to 30; changed to -50 mmol C m^{-2} d^{-1} during day 31 to 60; then to 100 mmol C m^{-2} d^{-1} during day 61 to 90; and to -50 mmol C m^{-2} d^{-1} during day 91 to 120 (Fig. 11a). The exponentially weighted NCP (NCP$_{weighted}$ in Fig. 11a) equals the O_2

5   bioflux derived from the O_2/Ar measurement (Teeter et al. 2018). Similar with Run-1, the air-sea O_2 flux quickly balanced the NCP-induced O_2 changes with a time lag of a few days after each change in NCP (Fig. 11c). However, the slow CO_2 gas exchange and the lingering background pCO_2 resulted in the decoupling between NCP and CO_2 flux (data in quadrant 1 and quadrant 3 in Fig. 11f). One typical example is the result during day 91 to 120: the strong preceding autotrophic production during days 61-90 led to low background pCO_2, which makes the seawater acted as a CO_2 sink under the heterotrophic

10   condition (Fig. 11).

In summary, the decoupling between NCP and CO_2 flux is a result of the competing effect of $\Delta pCO_{2background}$ and ΔpCO_{2NEP} in Eq. 15. In our observation, the surface waters with over-saturated pCO_2 and positive NCP were observed directly offshore of the Mississippi Southwest Pass (data in quadrant 1 in Fig. 9). This is the region where in situ autotrophic biological productivity began to increase due to the alleviated light limitation. However, the high background pCO_2 from the river

15   channel made the water still acted as a CO_2 source. Another case of decoupling between NCP and CO_2 flux was observed in the HTACW where CO_2 uptake occurred under heterotrophic conditions (data in quadrant 3 in Fig. 9). As discussed above, this phenomenon can be explained by benthic respiration-induced heterotrophy superimposed on advection of surface water with low background pCO_2 resulting from the preceding biological production (indicated by the negative values of ΔDIC_{NCP} and ΔNO_{xNCP} in Fig. 6e, f).

20   **Conclusions**

During a spring cruise in the norther Gulf of Mexico in April 2017, we found encouraging agreement among NCP estimates from multiple approaches despite the different temporal and spatial resolutions and uncertainties associated with different approaches. The O_2/Ar method has the advantage being able to provide high resolution NCP estimates matching the underway pCO_2 measurement, which allows a better examination on the coupling between NCP and CO_2 dynamics. The

variability of NCP and CO_2 showed higher spatial variability in inner and middle shelf strongly influenced by the Mississippi-Atchafalaya river system. Along the river-ocean mixing gradient, the availability of light generally determines the onset of the biological growth and the river-borne nutrient loading set the magnitude of the biological production. The surface NCP is characterized by low rates at both low-salinity end (light limitation) and high-salinity end (nutrient limitation), and high rates at intermediate salinities where light and nutrient are both favorable for phytoplankton growth. Due to the differences in the gas exchange rates of CO_2 and O_2, decoupling between NCP and CO_2 flux could be observed as the competing result of in situ production and the lingering effect of background pCO_2 of the source water.

References

Álvarez, M., Sanleón-Bartolomé, H., Tanhua, T., Mintrop, L., Luchetta, A., Cantoni, C., Schroeder, K., and Civitarese G.: The CO_2 system in the Mediterranean Sea: a basin wide perspective, Ocean Sci., 10(1), 69-92, https://doi.org/10.5194/os-10-69-2014, 2014.

Bauer, J. E., Cai, W. J., Raymond, P. A., Bianchi, T. S., Hopkinson, C. S., and Regnier, P. A. G.: The changing carbon cycle of the coastal ocean, Nature, 504, 61-70, https://doi.org/10.1038/nature12857, 2013.

Bianchi, T. S., DiMarco, S. F., Cowan, J. H., Hetland, R. D., Chapman, P., Day, J. W., and Allison, M. A.: The science of hypoxia in the Northern Gulf of Mexico: A review, Sci. Total Environ., 408, 1471-1484, https://doi.org/10.1016/j.scitotenv.2009.11.047, 2010.

Borges, A. V., and Abril, G.: Carbon dioxide and methane dynamics in estuaries, in: Treatise on estuarine and coastal science, edited by: Wolanski, E., and McLusky, D., Academic Press, Waltham, 119-161, https://doi.org/10.1016/B978-0-12-374711-2.00504-0, 2011.

Brewer, P. G., and Goldman, J. C.: Alkalinity changes generated by phytoplankton growth, Limnol. Oceanogr., 21, 108-117, https://doi.org/10.4319/lo.1976.21.1.0108, 1976.

Cai, W. J.: Riverine inorganic carbon flux and rate of biological uptake in the Mississippi River plume, Geophys. Res. Lett., 30, https://doi.org/10.1029/2002gl016312, 2003.

Cai, W. J., Dai, M. H., and Wang, Y. C.: Air-sea exchange of carbon dioxide in ocean margins: A province-based synthesis, Geophys. Res. Lett., 33, L12603, https://doi.org/10.1029/2006GL026219, 2006.

Cai, W. J.: Estuarine and coastal ocean carbon paradox: CO_2 sinks or sites of terrestrial carbon incineration?, Annual Review of Marine Science, Vol 3, 3, 123-145, https://doi.org/10.1146/annurev-marine-120709-142723, 2011.

Cai, W. J., Hu, X. P., Huang, W. J., Murrell, M. C., Lehrter, J. C., Lohrenz, S. E., Chou, W. C., Zhai, W. D., Hollibaugh, J. T., Wang, Y. C., Zhao, P. S., Guo, X. H., Gundersen, K., Dai, M. H., and Gong, G. C.: Acidification of subsurface coastal waters enhanced by eutrophication, Nature Geoscience, 4, 766-770, https://doi.org/10.1038/NGEO1297, 2011.

Cassar, N., Barnett, B. A., Bender, M. L., Kaiser, J., Hamme, R. C., and Tilbrook, B.: Continuous high-frequency dissolved O2/Ar measurements by equilibrator inlet mass spectrometry, Anal. Chem., 81, 1855-1864, https://doi.org/10.1021/ac802300u, 2009.

Cassar, N., DiFiore, P. J., Barnett, B. A., Bender, M. L., Bowie, A. R., Tilbrook, B., Petrou, K., Westwood, K. J., Wright, S. W., and Lefevre, D.: The influence of iron and light on net community production in the Subantarctic and Polar Frontal Zones, Biogeosciences, 8, 227-237, https://doi.org/10.5194/bg-8-227-2011, 2011.

Castro-Morales, K., Cassar, N., Shoosmith, D. R., and Kaiser, J.: Biological production in the Bellingshausen Sea from oxygen-to-argon ratios and oxygen triple isotopes, Biogeosciences, 10, 2273-2291, https://doi.org/10.5194/bg-10-2273-2013, 2013.

Chen, C.-T. A., and Borges, A. V.: Reconciling opposing views on carbon cycling in the coastal ocean: Continental shelves as sinks and near-shore ecosystems as sources of atmospheric CO_2, Deep Sea Res., Part II, 56, 578-590, https://doi.org/10.1016/j.dsr2.2009.01.001, 2009.

Chen, C.-T. A., Huang, T.-H., Fu, Y.-H., Bai, Y., and He, X.: Strong sources of CO_2 in upper estuaries become sinks of CO_2 in large river plumes, Curr. Opin. Environ. Sustain., 4, 179-185, https://doi.org/10.1016/j.cosust.2012.02.003, 2012.

Chen, C.-T. A., and Swaney, D. P.: Terrestrial-ocean transfers of carbon and nutrient across the coastal boundary: Editorial overview, Curr. Opin. Environ. Sustain., 4, 159-161, https://doi.org/10.1016/j.cosust.2012.03.001, 2012.

Chen, X., Lohrenz, S. E., and Wiesenburg, D. A.: Distribution and controlling mechanisms of primary production on the Louisiana–Texas continental shelf, J. Mar. Syst., 25, 179-207, http://dx.doi.org/10.1016/S0924-7963(00)00014-2, 2000.

Cooley, S. R., and Yager, P. L.: Physical and biological contributions to the western tropical North Atlantic Ocean carbon sink formed by the Amazon River plume, J. Geophys. Res., 111, https://doi.org/10.1029/2005JC002954, 2006.

Craig, H., and Hayward, T.: Oxygen supersaturation in the ocean: Biological versus physical contributions, Science, 235, 199-202, https://doi.org/10.1126/science.235.4785.199, 1987.

Dagg, M., Benner, R., Lohrenz, S., and Lawrence, D.: Transformation of dissolved and particulate materials on continental shelves influenced by large rivers: plume processes, Cont. Shelf Res., 24, 833-858, https://doi.org/10.1016/j.csr.2004.02.003, 2004.

Dickson, A. G., Sabine, C. L., and Christian, J. R.(Eds.): Guide to best practices for ocean CO_2 measurements, North Pacific Marine Science Organization (PICES), Sidney, British Columbia, 191 pp., 2007.

DeMaster, D. J., Smith, W. O., Nelson, D. M., and Aller, J. Y.: Biogeochemical processes in Amazon shelf waters: Chemical distributions and uptake rates of silicon, carbon and nitrogen, Cont. Shelf Res., 16, 617-643, https://doi.org/10.1016/0278-4343(95)00048-8, 1996.

Diaz, R. J., and Rosenberg, R.: Spreading dead zones and consequences for marine ecosystems, Science, 321, 926-929, https://doi.org/10.1126/science.1156401, 2008.

Egleston, E. S., Sabine, C. L., and Morel, F. M. M.: Revelle revisited: Buffer factors that quantify the response of ocean chemistry to changes in DIC and alkalinity, Global Biogeochem. Cycles, 24, https://doi.org/10.1029/2008GB003407, 2010.

Eppley, R. W., and Peterson, B. J.: Particulate organic matter flux and planktonic new production in the deep ocean, Nature, 282, 677-680, https://doi.org/10.1038/282677a0, 1979.

Fennel, K., Hetland, R., Feng, Y., and DiMarco, S.: A coupled physical-biological model of the Northern Gulf of Mexico shelf: model description, validation and analysis of phytoplankton variability, Biogeosciences, 8, 1881-1899, https://doi.org/10.5194/bg-8-1881-2011, 2011.

Garcia, H. E., and Gordon, L. I.: Oxygen solubility in seawater: Better fitting equations, Limnol. Oceanogr., 37, 1307-1312, https://doi.org/10.4319/lo.1992.37.6.1307, 1992.

Gattuso, J.-P, Frankignoulle, M., and Wollast, R.: Carbon and carbonate metabolism in coastal aquatic ecosystems, Annu. Rev. Ecol. Evol. Syst., 29, 405-434, https://doi.org/10.1146/annurev.ecolsys.29.1.405, 1998.

Geider, R. J., and La Roche, J.: Redfield revisited: variability of C:N:P in marine microalgae and its biochemical basis, Eur. J. Phycol., 37, 1-17, https://doi.org/10.1017/S0967026201003456, 2002.

Green, R. E., Bianchi, T. S., Dagg, M. J., Walker, N. D., and Breed, G. A.: An organic carbon budget for the Mississippi River turbidity plume and plume contributions to air-sea CO_2 fluxes and bottom water hypoxia, Estuaries and Coasts, 29, 579-597, https://doi.org/10.1007/BF02784284, 2006.

Guo, X., Cai, W.-J., Huang, W.-J., Wang, Y., Chen, F., Murrell, M. C., Lohrenz, S. E., Jiang, L.-Q., Dai, M., Hartmann, J., Lin, Q., and Culp, R.: Carbon dynamics and community production in the Mississippi River plume, Limnol. Oceanogr., 57, 1-17, https://doi.org/10.4319/lo.2012.57.1.0001, 2012.

Hamme, R. C., and Emerson, S. R.: The solubility of neon, nitrogen and argon in distilled water and seawater, Deep Sea Res., Part I, 51, 1517-1528, https://doi.org/10.1016/j.dsr.2004.06.009, 2004.

Hodur, R. M.: The Naval Research Laboratory's coupled ocean/Atmosphere Mesoscale Prediction System (COAMPS), Monthly Weather Review, 125, 1414-1430, https://doi.org/10.1175/1520-0493(1997)125<1414:TNRLSC>2.0.CO;2, 1997.

Huang, W. J., Cai, W. J., Powell, R. T., Lohrenz, S. E., Wang, Y., Jiang, L. Q., and Hopkinson, C. S.: The stoichiometry of inorganic carbon and nutrient removal in the Mississippi River plume and adjacent continental shelf, Biogeosciences, 9, 2781-2792, https://doi.org/10.5194/bg-9-2781-2012, 2012.

Huang, W. J., Cai, W. J., Castelao, R. M., Wang, Y. C., and Lohrenz, S. E.: Effects of a wind-driven cross-shelf large river plume on biological production and CO2 uptake on the Gulf of Mexico during spring, Limnol. Oceanogr., 58, 1727-1735, https://doi.org/10.4319/lo.2013.58.5.1727, 2013.

Huang, W. J., Cai, W. J., Wang, Y. C., Lohrenz, S. E., and Murrell, M. C.: The carbon dioxide system on the Mississippi River-dominated continental shelf in the northern Gulf of Mexico: 1. Distribution and air-sea CO_2 flux, J. Geophys. Res., 120, 1429-1445, https://doi.org/10.1002/2014JC010498, 2015.

Jonsson, B. F., Doney, S. C., Dunne, J., and Bender, M.: Evaluation of the Southern Ocean O2/Ar-based NCP estimates in a model framework, J. Geophys. Res., 118, 385-399, https://doi.org/10.1002/jgrg.20032, 2013.

Justić, D., Rabalais, N. N., Eugene Turner, R., and Wiseman, W. J.: Seasonal coupling between riverborne nutrients, net productivity and hypoxia, Mar. Pollut. Bull., 26, 184-189, http://dx.doi.org/10.1016/0025-326X(93)90620-Y, 1993.

5 Kaiser, J., Reuer, M. K., Barnett, B., and Bender, M. L.: Marine productivity estimates from continuous O_2/Ar ratio measurements by membrane inlet mass spectrometry, Geophys. Res. Lett., 32, https://doi.org/10.1029/2005gl023459, 2005.

Laruelle, G. G., Durr, H. H., Slomp, C. P., and Borges, A. V.: Evaluation of sinks and sources of CO2 in the global coastal ocean using a spatially-explicit typology of estuaries and continental shelves, Geophys. Res. Lett., 37,

10 https://doi.org/10.1029/2010gl043691, 2010.

Laws, E. A.: Photosynthetic quotients, new production and net community production in the open ocean, Deep-Sea Research Part a-Oceanographic Research Papers, 38, 143-167, https://doi.org/10.1016/0198-0149(91)90059-O, 1991.

Lawson, C. L., and Hanson, R. J. (Eds.): Solving Least Squares Problems, Prentice-Hall, Chapter 23, 161 pp., 1974.

Lehrter, J. C., Ko, D. S., Murrell, M. C., Hagy, J. D., Schaeffer, B. A., Greene, R. M., Gould, R. W., and Penta, B.: Nutrient

15 distributions, transports, and budgets on the inner margin of a river-dominated continental shelf, J. Geophys. Res., 118, 4822-4838, https://doi.org/10.1002/jgrc.20362, 2013.

Lehrter, J. C., Murrell, M. C., and Kurtz, J. C.: Interactions between freshwater input, light, and phytoplankton dynamics on the Louisiana continental shelf, Cont. Shelf Res., 29, 1861-1872, http://dx.doi.org/10.1016/j.csr.2009.07.001, 2009.

Liss, P. S., and Merlivat, L.: Air-sea gas exchange rates: Introduction and synthesis, in: The role of air-sea exchange in

20 geochemical cycling, edited by: Buat-Menard, P., D. Reidel, Hingham, Mass., 1986.

Lohrenz, S. E., Dagg, M. J., and Whitledge, T. E.: Enhanced primary production at the plume pceanic interface of the Mississippi River, Cont. Shelf Res., 10, 639-664, https://doi.org/10.1016/0278-4343(90)90043-L, 1990.

Lohrenz, S. E., Fahnenstiel, G. L., Redalje, D. G., Lang, G. A., Chen, X. G., and Dagg, M. J.: Variations in primary production of northern Gulf of Mexico continental shelf waters linked to nutrient inputs from the Mississippi River, Mar.

25 Ecol. Prog. Ser., 155, 45-54, https://doi.org/10.3354/meps155045, 1997.

Lohrenz, S. E., Fahnenstiel, G. L., Redalje, D. G., Lang, G. A., Dagg, M. J., Whitledge, T. E., and Dortch, Q.: Nutrients, irradiance, and mixing as factors regulating primary production in coastal waters impacted by the Mississippi River plume, Cont. Shelf Res., 19, 1113-1141, http://dx.doi.org/10.1016/S0278-4343(99)00012-6, 1999.

Lohrenz, S. E., Cai, W.-J., Chen, F., Chen, X., and Tuel, M.: Seasonal variability in air-sea fluxes of CO_2 in a river-

30 influenced coastal margin, Journal of Geophysical Research: Oceans, 115, https://doi.org/10.1029/2009JC005608, 2010.

Lohrenz, S. E., Cai, W. J., Chakraborty, S., Gundersen, K., and Murrell, M. C.: Nutrient and carbon dynamics in a large river-dominated coastal ecosystem: the Mississippi-Atchafalaya River system, in: Biogeochemical dynamics at major river-coastal interfaces: Linkages with global change, edited by: Bianchi, T. S., Allison, M. A., and Cai, W.-J., 48-472, http://dx.doi.org/10.1017/CBO9781139136853.023, 2014.

McKee, B. A., Aller, R. C., Allison, M. A., Bianchi, T. S., and Kineke, G. C.: Transport and transformation of dissolved and particulate materials on continental margins influenced by major rivers: benthic boundary layer and seabed processes, Cont. Shelf Res., 24, 899-926, http://dx.doi.org/10.1016/j.csr.2004.02.009, 2004.

Muller-Karger, F. E., Varela, R., Thunell, R., Luerssen, R., Hu, C. M., and Walsh, J. J.: The importance of continental margins in the global carbon cycle, Geophys. Res. Lett. 32, http://dx.doi.org/10.1029/2004gl021346, 1, 2005.

Murrell, M. C., Stanley, R. S., Lehrter, J. C., and Hagy, J. D.: Plankton community respiration, net ecosystem metabolism, and oxygen dynamics on the Louisiana continental shelf: Implications for hypoxia, Cont. Shelf Res., 52, 27-38, https://doi.org/10.1016/j.csr.2012.10.010, 2013.

Nicholson, D. P., Stanley, R. H. R., Barkan, E., Karl, D. M., Luz, B., Quay, P. D., and Doney, S. C.: Evaluating triple oxygen isotope estimates of gross primary production at the Hawaii Ocean Time-series and Bermuda Atlantic Time-series Study sites, J. Geophys. Res., 117, https://doi.org/10.1029/2010jc006856, 2012.

Nightingale, P. D., Malin, G., Law, C. S., Watson, A. J., Liss, P. S., Liddicoat, M. I., Boutin, J., and Upstill-Goddard, R. C.: In situ evaluation of air-sea gas exchange parameterizations using novel conservative and volatile tracers, Global Biogeochem. Cycles, 14, 373-387, https://doi.org/10.1029/1999GB900091, 2000.

Ning, X. R., Vaulot, D., Liu, Z. S., and Liu, Z. L.: Standing stock and production of phytoplankton in the estuary of the Changjiang (Yangtse River) and the adjacent East China Sea, Mar. Ecol. Prog. Ser., 49, 141-150, https://doi.org/10.3354/meps049141, 1988.

Obenour, D. R., Scavia, D., Rabalais, N. N., Turner, R. E., and Michalak, A. M.: Retrospective analysis of midsummer hypoxic area and volume in the Northern Gulf of Mexico, 1985–2011, Environ. Sci. Technol., 47, 9808-9815, https://doi.org/10.1021/es400983g, 2013.

Pai, S.-C., Gong, G.-C., and Liu, K.-K.: Determination of dissolved oxygen in seawater by direct spectrophotometry of total iodine, Mar. Chem., 41, 343-351, http://dx.doi.org/10.1016/0304-4203(93)90266-Q, 1993.

Pierrot, D., Lewis, E., and Wallace, D. W. R.: MS Excel program developed for CO_2 system Calculations, ORNL/CDIAC-105a. Carbon Dioxide Information Analysis Center, Oak Ridge National Laboratory, US Department of Energy, Oak Ridge, TN, https://doi.org/10.3334/CDIAC/otg.CO2SYS_XLS_CDIAC105a, 2006.

Rabalais, N. N., Turner, R. E., and Wiseman, W. J.: Gulf of Mexico hypoxia, aka "The dead zone", Annu. Rev. Ecol. Syst., 33, 235-263, https://doi.org/10.1146/annurev.ecolsys.33.010802.150513, 2002.

Rabalais, N. N., Cai, W. J., Carstensen, J., Conley, D. J., Fry, B., Hu, X. P., Quinones-Rivera, Z., Rosenberg, R., Slomp, C. P., Turner, R. E., Voss, M., Wissel, B., and Zhang, J.: Eutrophication-driven deoxygenation in the coastal ocean, Oceanography, 27, 172-183, https://doi.org/10.5670/oceanog.2014.21, 2014.

Regnier, P., Friedlingstein, P., Ciais, P., Mackenzie, F. T., Gruber, N., Janssens, I. A., Laruelle, G. G., Lauerwald, R., Luyssaert, S., Andersson, A. J., Arndt, S., Arnosti, C., Borges, A. V., Dale, A. W., Gallego-Sala, A., Godderis, Y., Goossens, N., Hartmann, J., Heinze, C., Ilyina, T., Joos, F., LaRowe, D. E., Leifeld, J., Meysman, F. J. R., Munhoven, G.,

Raymond, P. A., Spahni, R., Suntharalingam, P., and Thullner, M.: Anthropogenic perturbation of the carbon fluxes from land to ocean, Nature Geoscience, 6, 597-607, https://doi.org/10.1038/ngeo1830, 2013.

Reuer, M. K., Barnett, B. A., Bender, M. L., Falkowski, P. G., and Hendricks, M. B.: New estimates of Southern Ocean biological production rates from O_2/Ar ratios and the triple isotope composition of O_2, Deep Sea Res., Part I, 54, 951-
5   974, https://doi.org/10.1016/j.dsr.2007.02.007, 2007.

Roberts, B. J., and Doty, S. M.: Spatial and temporal patterns of benthic respiration and net nutrient fluxes in the Atchafalaya River Delta Estuary, Estuaries and Coasts, 38, 1918-1936, https://doi.org/10.1007/s12237-015-9965-z, 2015.

Sambrotto, R. N., Savidge, G., Robinson, C., Boyd, P., Takahashi, T., Karl, D. M., Langdon, C., Chipman, D., Marra, J., and
10   Codispoti, L.: Elevated consumption of carbon relative to nitrogen in the surface ocean, Nature, 6426, https://doi.org/10.1038/363248a0, 1993.

Sarmiento, J. L., and Gruber, N. (Eds.): Ocean Biogeochemical Dynamics, Princeton University Press, Princeton, NJ, 528 pp., 2006.

Shadwick, E. H., Tilbrook, B., Cassar, N., Trull, T. W., and Rintoul, S. R.: Summertime physical and biological controls on
15   O_2 and CO_2 in the Australian Sector of the Southern Ocean, J. Mar. Syst., 147, 21-28, https://doi.org/10.1016/j.jmarsys.2013.12.008, 2015.

Sweeney, C., Gloor, E., Jacobson, A. R., Key, R. M., McKinley, G., Sarmiento, J. L., and Wanninkhof, R.: Constraining global air-sea gas exchange for CO_2 with recent bomb ^{14}C measurements, Global Biogeochem. Cycles, 21, GB2015, https://doi.org/10.1029/2006gb002784, 2007.

20   Teeter, L., Hamme, R. C., Ianson, D., and Bianucci, L.: Accurate etimation of nt cmmunity poduction gom O_2/Ar masurements, Global Biogeochem. Cycles, 32, 1163-1181, https://doi.org/10.1029/2017GB005874, 2018.

Ternon, J. F., Oudot, C., Dessier, A., and Diverres, D.: A seasonal tropical sink for atmospheric CO_2 in the Atlantic ocean: the role of the Amazon River discharge, Mar. Chem., 68, 183-201, https://doi.org/10.1016/s0304-4203(99)00077-8, 2000.

Turner, R. E., Rabalais, N. N., and Justic, D.: Predicting summer hypoxia in the northern Gulf of Mexico: Redux, Mar.
25   Pollut. Bull., 64, 319-324, https://doi.org/10.1016/j.marpolbul.2011.11.008, 2012.

Turner, R. E., and Rabalais, N. N.: Nitrogen and phosphorus phytoplankton growth limitation in the northern Gulf of Mexico, Aquat. Microb. Ecol., 68, 159-169, https://doi.org/10.3354/ame01607, 2013.

Ulfsbo, A., Cassar, N., Korhonen, M., van Heuven, S., Hoppema, M., Kattner, G., and Anderson, L. G.: Late summer net community production in the central Arctic Ocean using multiple approaches, Global Biogeochem. Cycles, 28, 1129-
30   1148, https://doi.org/10.1002/2014GB004833, 2014.

Wallace, R. B., Baumann, H., Grear, J. S., Aller, R. C., and Gobler, C. J.: Coastal ocean acidification: The other eutrophication problem, Estuarine, Coastal Shelf Sci., 148, 1-13, https://doi.org/10.1016/j.ecss.2014.05.027, 2014.

Wanninkhof, R.: Relationship between wind-speed and gas-exchange over the ocean, J. Geophys. Res., 97, 7373-7382, https://doi.org/10.1029/92jc00188, 1992.

Weiss, R. F. (Eds.): Carbon dioxide in water and seawater: the solubility of a non-ideal gas. In: Mar. Chem., 1974.

Wolf-Gladrow, D. A., Zeebe, R. E., Klaas, C., Kortzinger, A., and Dickson, A. G.: Total alkalinity: The explicit conservative expression and its application to biogeochemical processes, Mar. Chem., 106, 287-300, https://doi.org/10.1016/j.marchem.2007.01.006, 2007.

5   Xue, J. H., Cai, W. J., Hu, X. P., Huang, W. J., Lohrenz, S. E., and Gundersen, K.: Temporal variation and stoichiometric ratios of organic matter remineralization in bottom waters of the northern Gulf of Mexico during late spring and summer, J. Geophys. Res., 120, 8304-8326, https://doi.org/10.1002/2015JC011453, 2015.

Xue, Z., He, R., Fennel, K., Cai, W. J., Lohrenz, S., and Hopkinson, C.: Modeling ocean circulation and biogeochemical variability in the Gulf of Mexico, Biogeosciences, 10, 7219-7234, https://doi.org/10.5194/bg-10-7219-2013, 2013.

10 Xue, Z., He, R. Y., Fennel, K., Cai, W. J., Lohrenz, S., Huang, W. J., Tian, H. Q., Ren, W., and Zang, Z. C.: Modeling pCO$_2$ variability in the Gulf of Mexico, Biogeosciences, 13, 4359-4377, https://doi.org/10.5194/bg-13-4359-2016, 2016.

Yang, X. F., Xue, L., Li, Y. X., Han, P., Liu, X. Y., Zhang, L. J., and Cai, W. J.: Treated wastewater changes the export of dissolved inorganic carbon and its isotopic composition and leads to acidification in coastal oceans, Environ. Sci. Technol., 52, 5590-5599, https://doi.org/10.1021/acs.est.8b00273, 2018.

15 Zeebe, R. E., and D. Wolf-Gladrow (Eds.): CO$_2$ in seawater: Equilibrium, kinetics, isotopes., Elsevier, Amsterdam, 2001.

Zhang, X. Q., Hetland, R. D., Marta-Almeida, M., and DiMarco, S. F.: A numerical investigation of the Mississippi and Atchafalaya freshwater transport, filling and flushing times on the Texas-Louisiana Shelf, J. Geophys. Res., 117, https://doi.org/10.1029/2012jc008108, 2012.
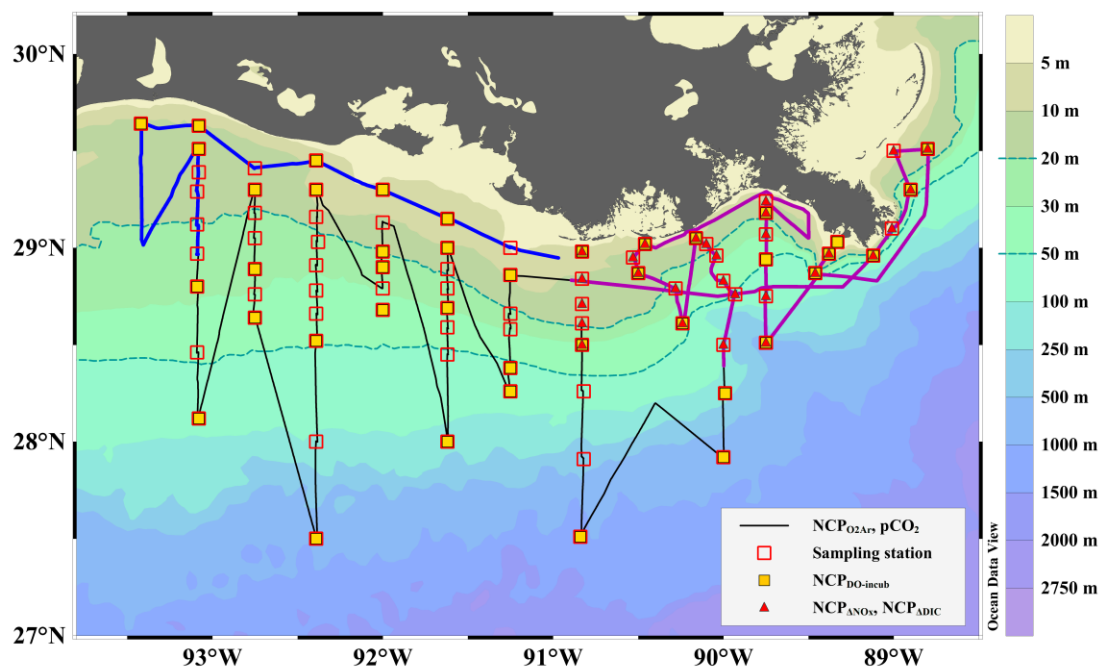
Table

Table 1 The end member properties used in the three end-member mixing model.

End member	Salinity	TA (μmol kg^{-1})	DIC (μmol kg^{-1})	NO$_x$ (μmol kg^{-1})
Atchafalaya	0	2090.58	2128.15	113.14
Mississippi	0	2314.43	2312.28	123.27
Gulf surface	36.15	2406.98	2076.34	0.44

Figure

5

Figure 1: The underway measurements (black lines), sampling stations (red squares), stations where light/dark bottle DO incubations were conducted (yellow squares), and stations where non-conservative changes in DIC and NO$_x$ were used to estimate net community production (NCP) rates in the Mississippi plume (red triangles). The 20 m and 50 m isobaths are highlighted, as well as the cruise track in the Mississippi plume (purple, Apr. 8-10) and the Atchafalaya coast (blue, Apr. 15-17).

10
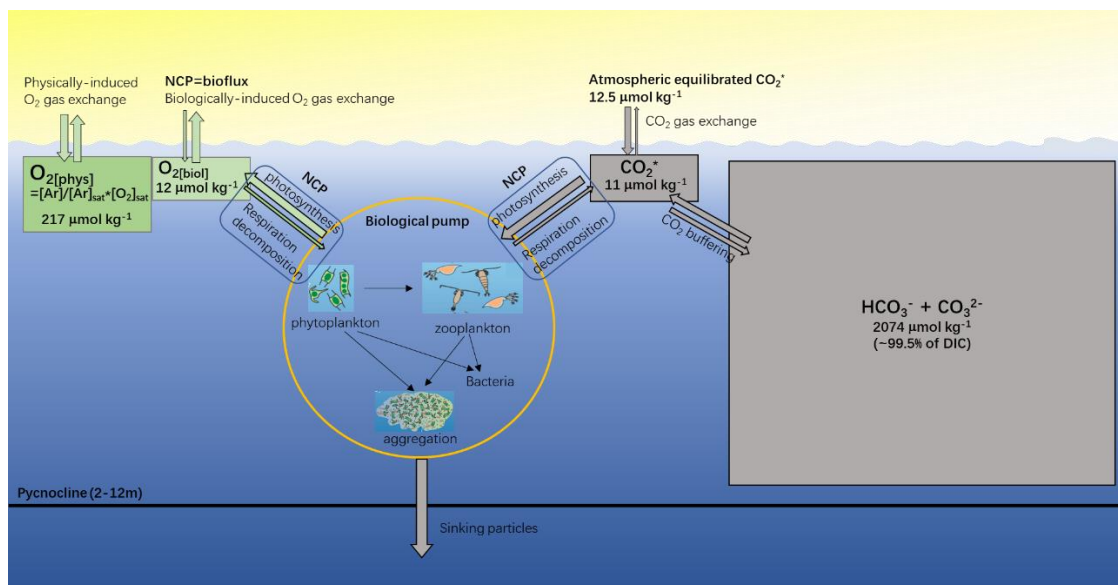
Figure 2: Schematic of the relationships of the surface NCP and air-sea gas exchange of O_2 and CO_2. The green and grey boxes refer to the reservoirs of O_2 and CO_2 in the mixed layer, and green and grey arrows refer to the O_2 and CO_2 fluxes respectively. The values shown in the figure were calculated under the mean surface condition during the cruise in April 2017

5 **(temperature=22°C, salinity=35, DO=228 µmol kg^{-1}, DIC=2075 µmol kg^{-1}, TA=2400 µmol kg^{-1}). Under a steady state assumption in the mixed layer, the surface NCP can be approximated by the O_2 bioflux (biologically-induced air-sea O_2 exchange flux) estimated from the O_2/Ar measurement (see the text for details). The longer equilibrium time of CO_2 (compared to that of O_2) is due to the different gas exchange rates of the two gases and the buffering effect of the CO_2^*-HCO_3^--CO_3^{2-} system, where CO_2^* refers to the aquatic CO_2 and H_2CO_3.**
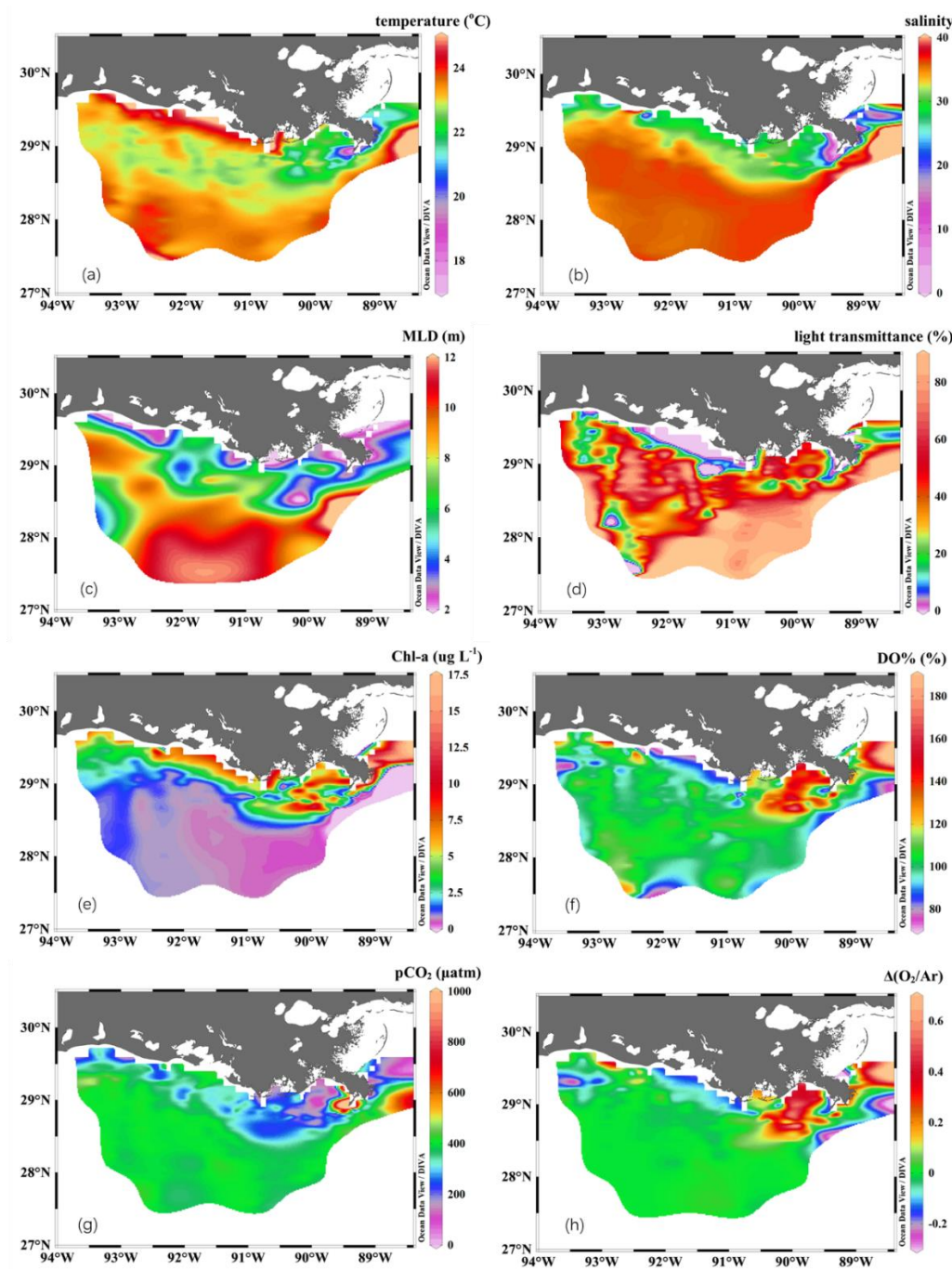
Figure 3: The distribution of (a) temperature, (b) salinity, (c) mixed layer depth (MLD), (d) light transmittance, (e) Chl-a, (f) percentage saturation of oxygen (DO%), (g) partial pressure of CO₂ (*p*CO₂), and (h) biological-induced oxygen supersaturation (ΔO₂/Ar) in the surface water in the nGOM.
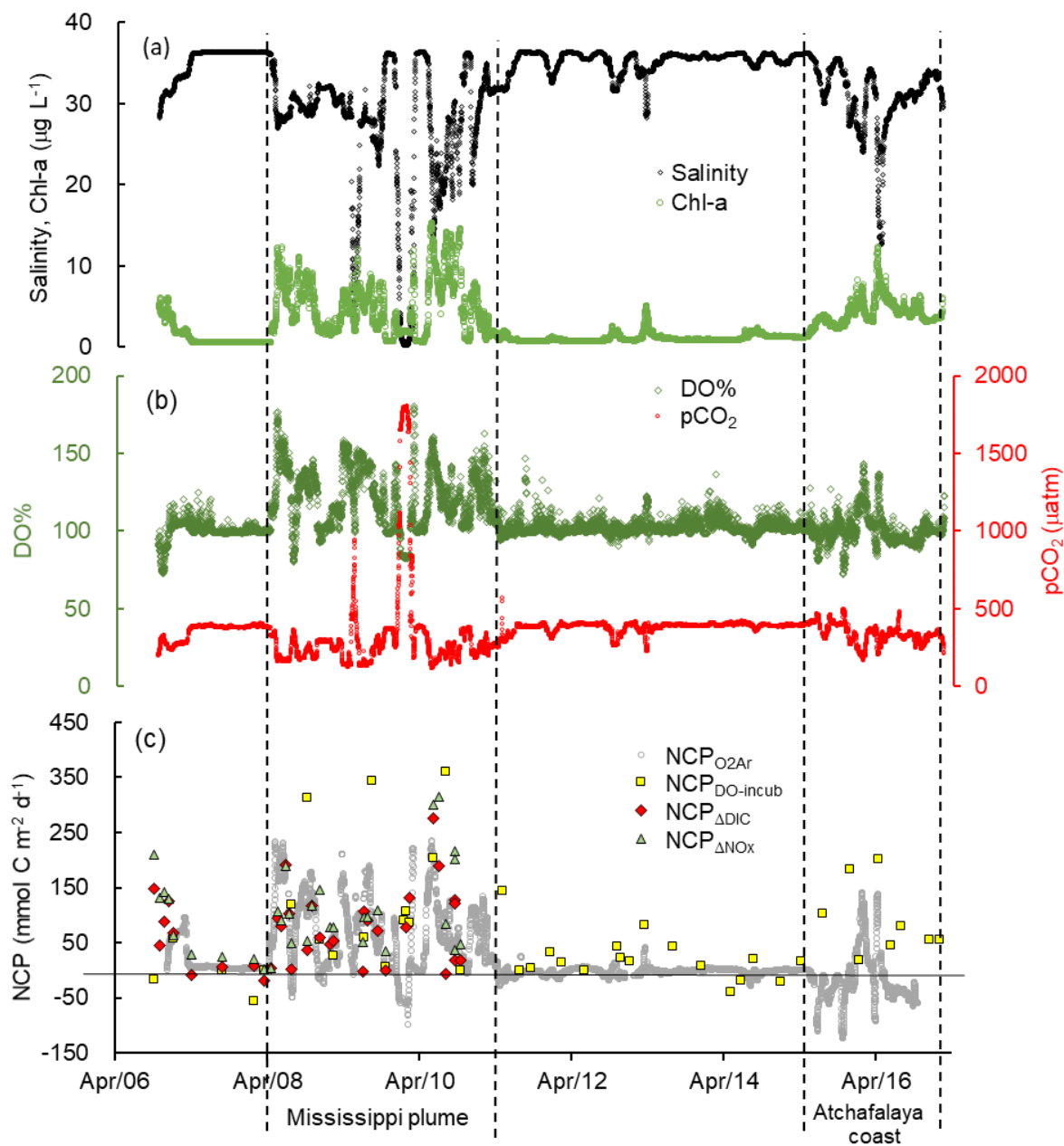
Figure 4: The underway measurements of (a) salinity and Chl-a, (b) DO% and pCO$_2$ and (c) mixed layer average NCP rates from the O$_2$/Ar measurement (NCP$_{O2Ar}$, gray circles). Also shown in panel c are the NCP rates estimated from the light/dark DO incubation (NCP$_{DO-incub}$, yellow squares), non-conservative changes in DIC (NCP$_{\Delta DIC}$, red diamonds) or NO$_x$ (NCP$_{\Delta NOx}$, green triangles). See Figure 1 for the cruise track in the Mississippi plume (Apr. 8-10) and Atchafalaya coast (Apr. 15-17).
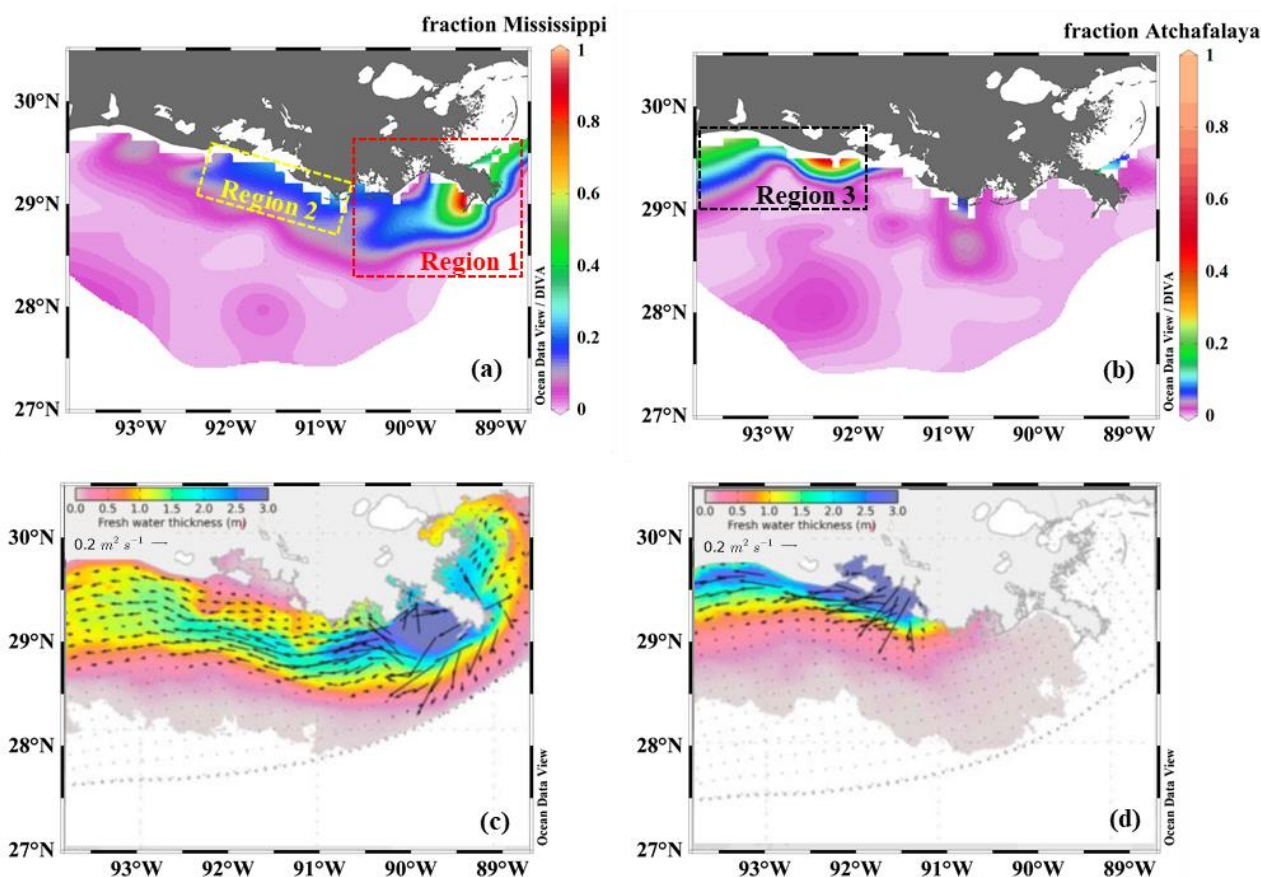
Figure 5 The fractional contribution of the (a) Mississippi and (b) Atchafalaya to the surface water in the nGOM estimated from the three end-member mixing model. The multiple-year average of freshwater thickness and transport of the (c) Mississippi and (d) Atchafalaya from a high resolution coastal model by Zhang et al. (2012). The sub-regions are shown in panel (a) and (b): 1) Mississippi plume, 2) high-turbidity Atchafalaya coastal water (HTACW), and 3) Atchafalaya plume. Panels (c) and (d) are reproduced from Zhang et al. (2012).
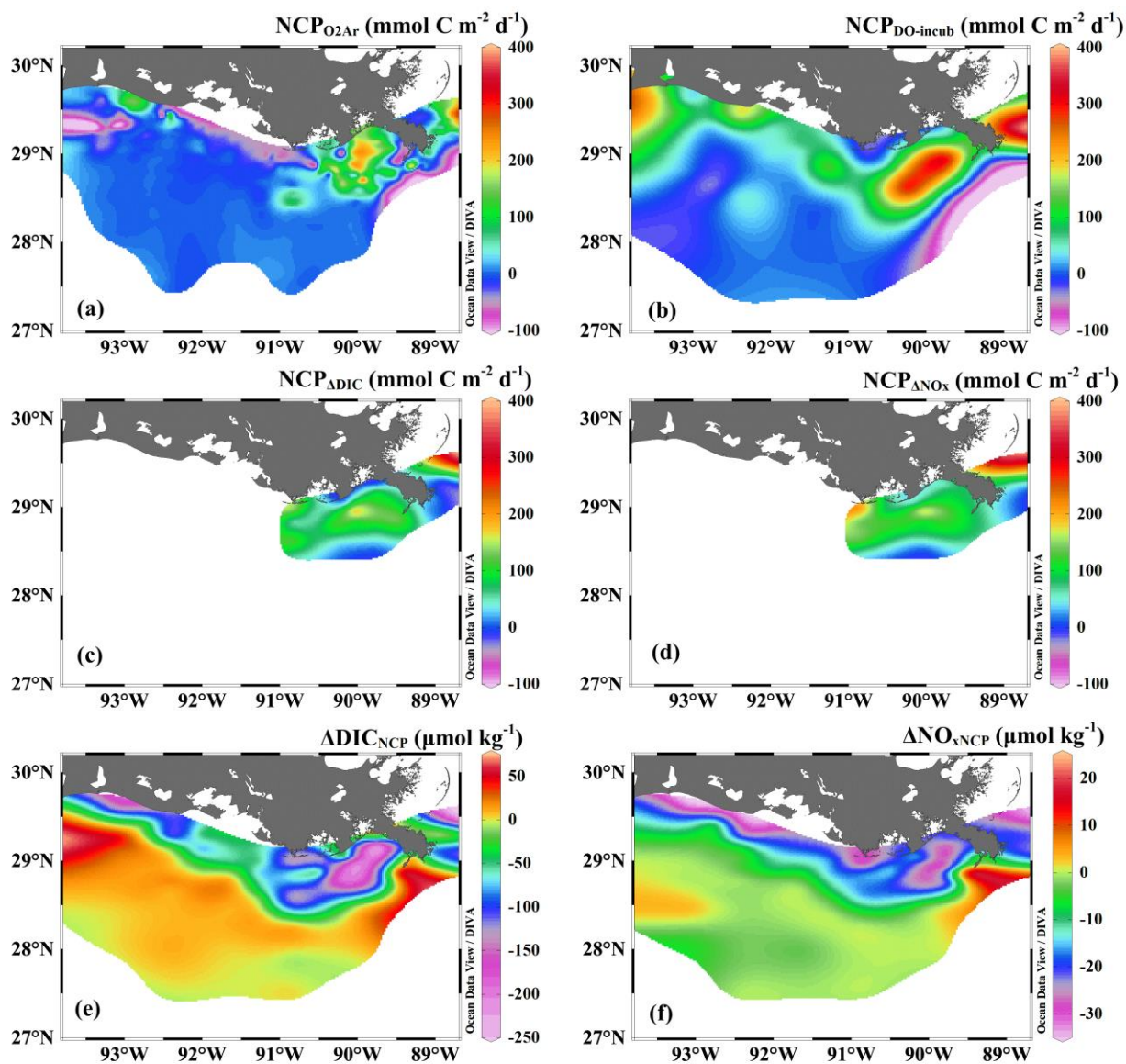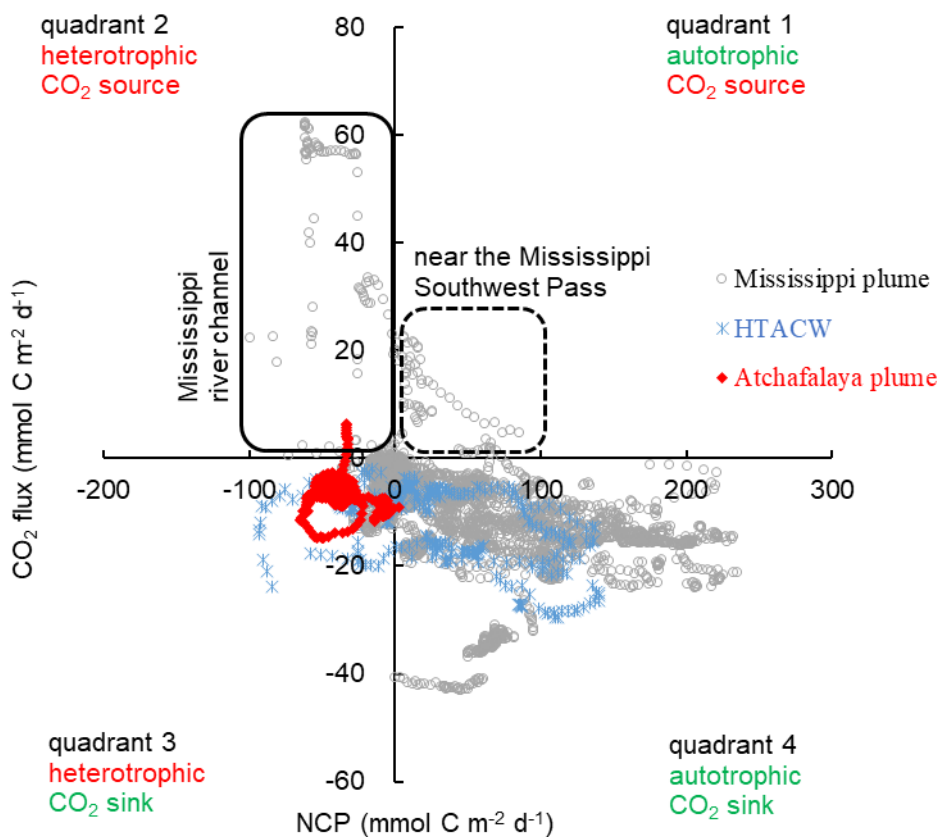
Figure 6: The distribution of the mixed layer average (a) NCP$_{O2Ar}$, (b) NCP$_{DO-incub}$, (c) NCP$_{\Delta DIC}$, (d) NCP$_{\Delta NOx}$, (e) cumulative NCP-induced changes in DIC (ΔDIC_{NCP}) and (f) cumulative NCP-induced changes in NO$_x$ (ΔNO_{xNCP}). Noted that NCP$_{\Delta DIC}$ and NCP$_{\Delta NOx}$ were only estimated in the Mississippi plume (panel c, d).

5
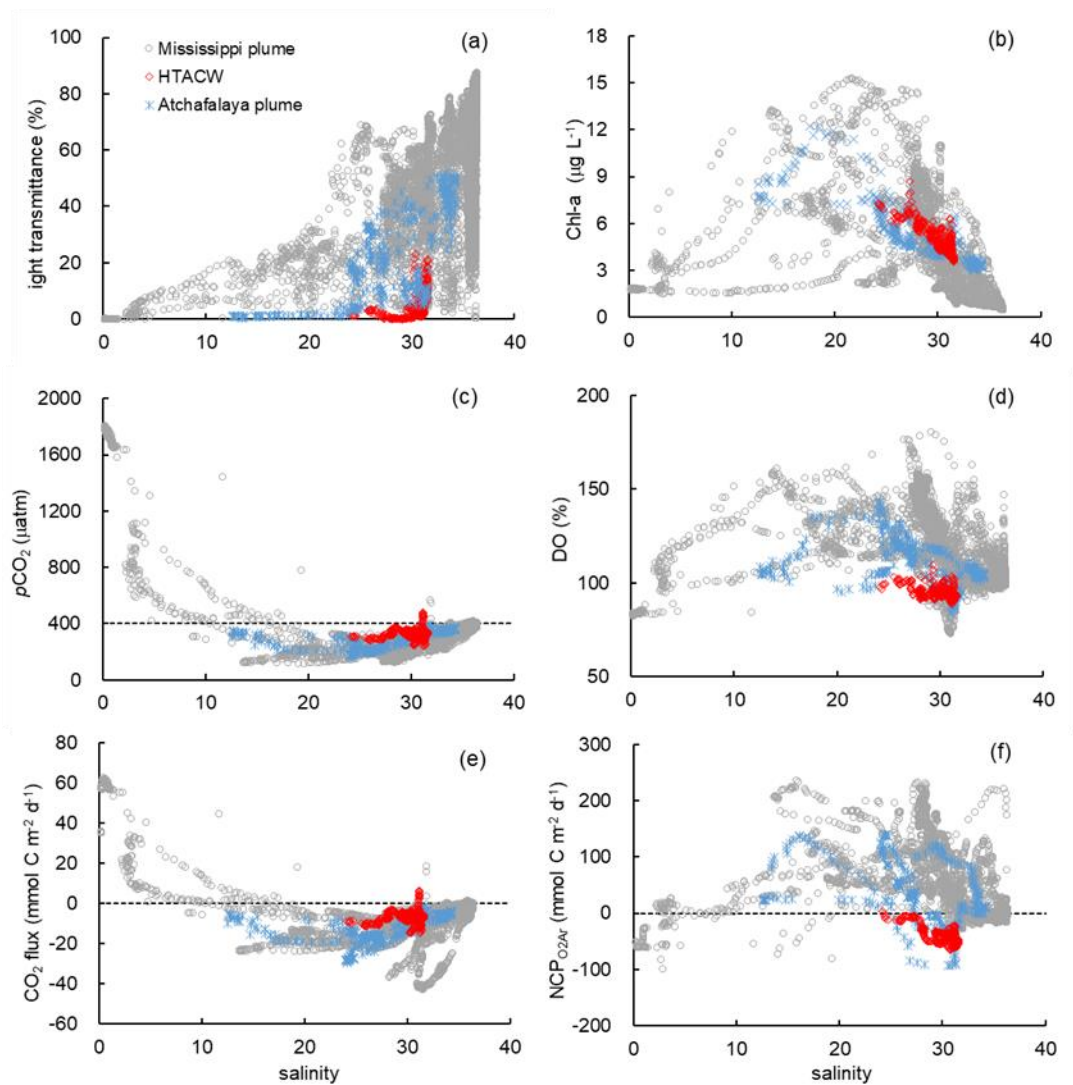
Figure 7: The distribution of (a) light transmittance, (b) Chl-a, (c) pCO_2, (d) DO%, (e) CO_2 flux and (f) NCP_{O2Ar} along the salinity gradient in the three sub-regions (*see* Fig. 5a, b). The dash line in panel c is the atmospheric pCO_2 (405 μatm).
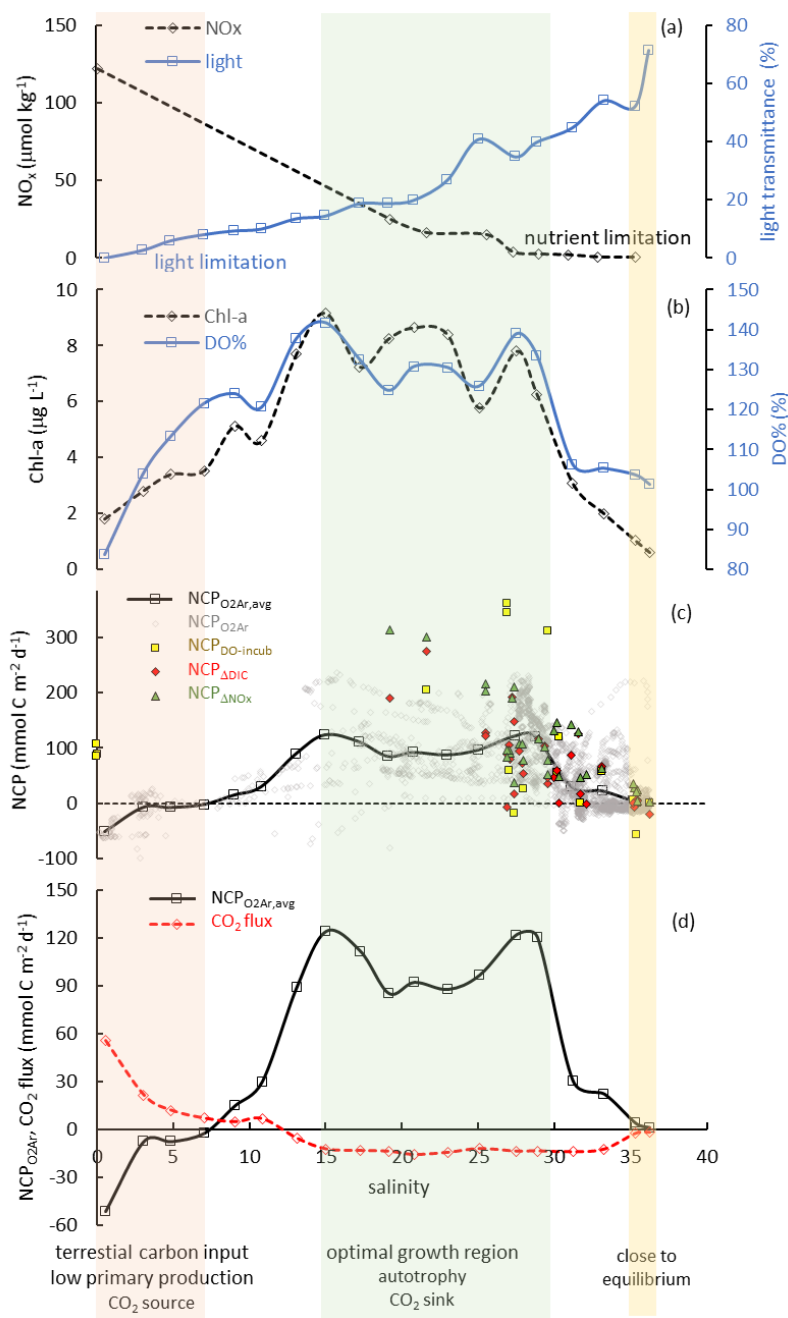
Figure 8: The distribution of averaged (a) NO_x and light transmittance, (b) Chl-a and DO%, (c) $NCP_{O2Ar,avg}$ and (d) $NCP_{O2Ar,avg}$ and CO_2 flux along the salinity gradient in the surface water of the Mississippi plume (region 1 in Fig. 5a). Data were averaged over increments of two salinity units. Also shown in panel c are the NCP rates estimated from the light/dark DO incubation

5 ($NCP_{DO-incub}$, yellow squares), non-conservative changes in DIC ($NCP_{\Delta DIC}$, red diamonds) or NO_x ($NCP_{\Delta NOx}$, green triangles).

Figure 9: The scatter plot of NCP$_{O2Ar}$ and CO$_2$ flux in the nGOM. Positive NCP implies net organic carbon production (autotrophy) and negative CO$_2$ flux implies net CO$_2$ uptake from the atmosphere (oceanic CO$_2$ sink).
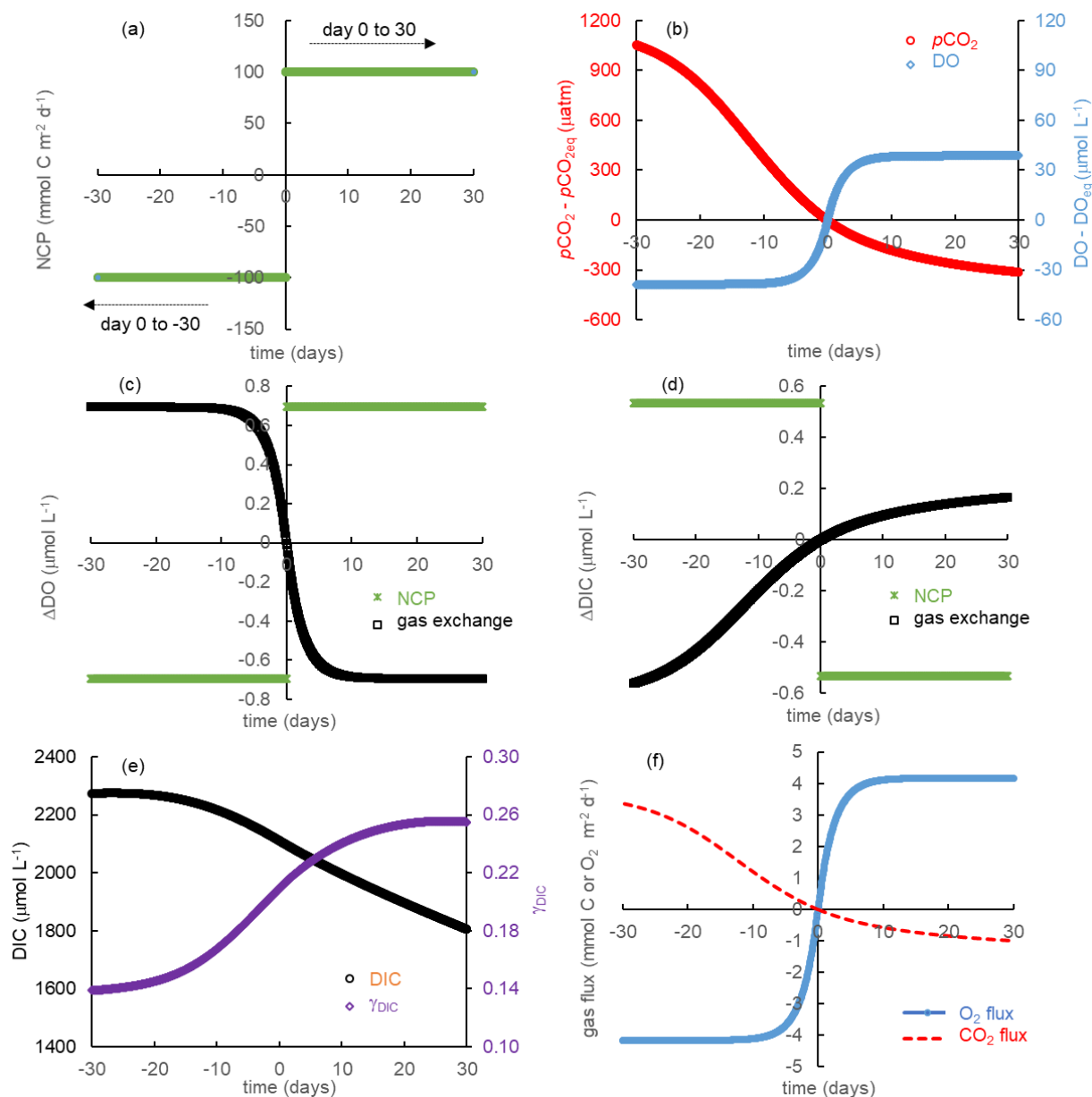
Figure 10 Simulation of carbon and oxygen dynamics responding to NCP and gas exchange using a 1-D model. The water is assumed to be equilibrium with atmosphere at day 0, autotrophic production occurs from day 0 to day 30 while heterotrophic production occurs from day 0 to day -30. The variations of (a) NCP, (b) the deviation of pCO_2 and DO from equilibrium (pCO_2-pCO_{2eq} and DO-DO$_{eq}$), (c) DO changes resulting from NCP and gas exchange, (d) DIC changes resulting from NCP and gas exchange, (e) DIC and pCO_2 buffering factor (γ_{DIC}), and (f) O$_2$ flux and CO$_2$ flux.
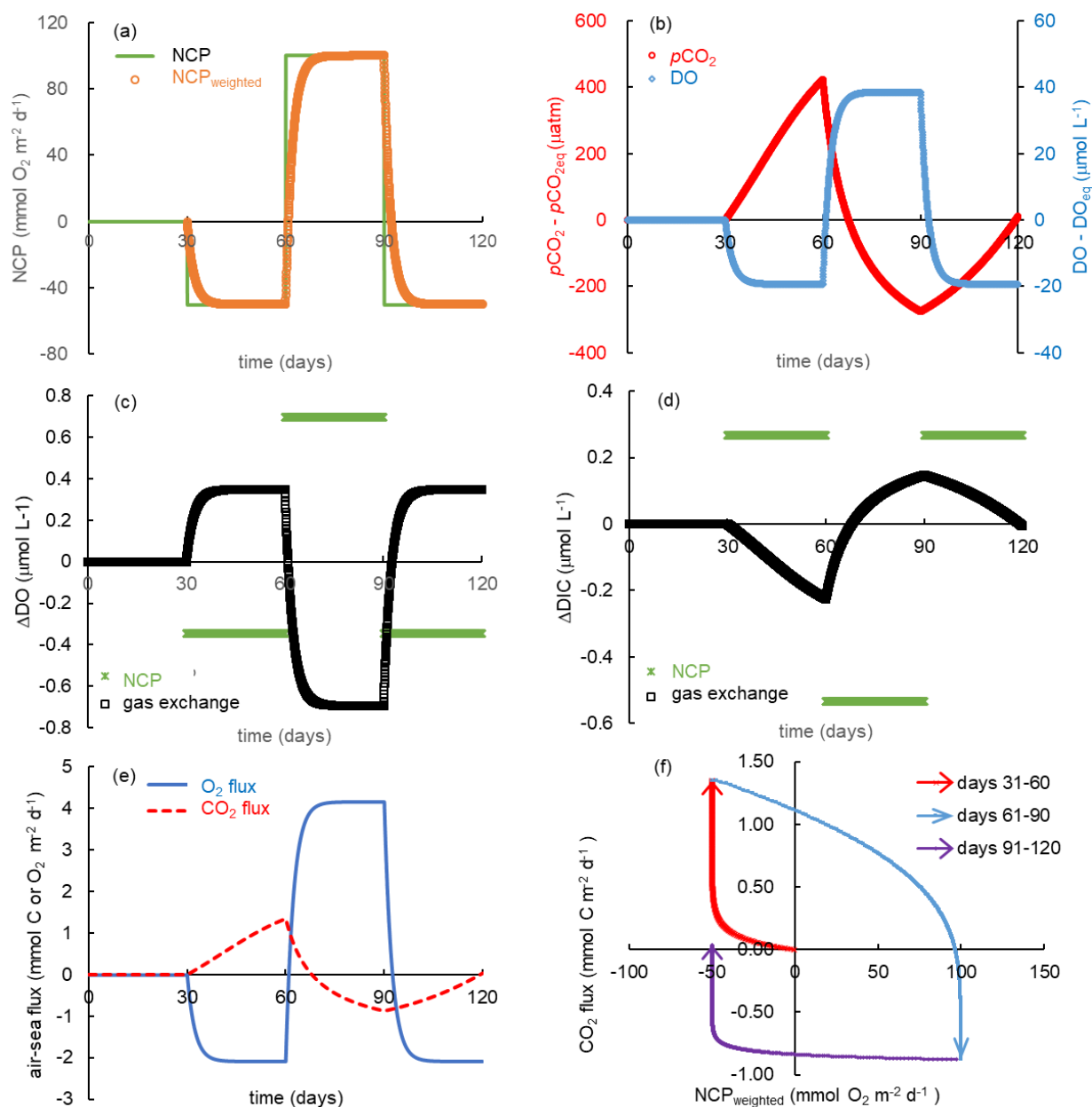
Figure 11: Simulation of carbon and oxygen dynamics responding to NCP and gas exchange using a 1-D model. The water is assumed to be equilibrium with atmosphere at day 0, autotrophic production occurs during days 31 to 60 and days 91 to 120, heterotrophic production occurs during days 61 to 90. The variations of (a) NCP and exponentially weighted NCP (NCP_weighted), (b) the deviation of pCO$_2$ and DO from equilibrium, (c) DO changes resulting from NCP and gas exchange, (d) DIC changes resulting from NCP and gas exchange, and (e) O$_2$ flux and CO$_2$ flux. (f) The scatter plot of CO$_2$ flux and NCP_weighted.